공학석사 학위논문

상처 드레싱을 위한 생활성 코팅 보조제로서의 접착성 코아세르베이트

Adhesive coacervate as a bioactive coating supplement for wound dressings

2023년 2월

서울대학교 대학원

응용바이오공학과

김 영

상처 드레싱을 위한 생활성 코팅 보조제로서의 접착성 코아세르베이트

Adhesive coacervate as a bioactive coating supplement for wound dressings

지도 교수 이 강 원

이 논문을 공학석사 학위논문으로 제출함
2023년 1 월

서울대학교 대학원
응용바이오공학과
김 영

김 영의 공학석사 학위논문을 인준함
2023 년 1 월

위 원 장 _____ (인)

부위원장 _____ (인)

위 원 _____ (인)

Abstract

Adhesive coacervate as a bioactive coating supplement for wound dressings

Young Kim

Department of Applied bioengineering

Graduate School of Convergence Science and Technology

Seoul National University

Wound healing using growth factors is a clinically effective treatment method. However, it has a short biological half-life due to protease secreted into the wound area to break down the damaged extracellular matrix (ECM). The study shows a new coating supplement functionalizing adhesiveness using dopamine (DOPA) to the complex coacervate of fucoidan and poly-*l*-lysine (PLL), showing antioxidant properties that useful in wound healing. The dopamine-complex coacervate (D-Coa) was optimized to form maximum micro-droplets. The D-Coa, dopamine functionalized fucoidan, a marine-derived glycosaminoglycan, and poly-*l*-lysine (PLL) coacervates have shown promising protein delivery; sustained release profile, superior

encapsulation ability, biocompatibility, and protection against harsh *in-vivo* environment, for tissue engineering applications as our previous fucoidan and poly-l-lysine (PLL) complex coacervate study was shown. Furthermore, the D-Coa was conducted superior adhesive forces and successfully coated onto collagen sponge homogeneously and rapidly. From *in vivo* performance tests using at skin defect models, our D-Coa coating patch were demonstrated successful wound regeneration. This game changer coating supplements can rescue biological half-life and reduce coating time, preventing limited application of scaffold such as commercially available collagen sponge.

Keyword : Coacervate, DOPA, Coating, Drug Delivery System(DDS), sustained release profile

Student Number : 2021-22766

Table of Contents

List of Figures

Chapter 1. Introduction

Acute wound is a common skin injury which occurs approximately 11 million incidents with 300,000 hospitalized patients per annum in the United States.[1] In addition, the wound healing medical devices market is growing exponentially every year, and research to enhance the current wound healing products is being actively conducted.[2, 3] The wound is usually caused by trauma and burns.[4] Without a prompt treatment, the general wound healing process, such as hemostasis, inflammation, proliferation, and remodeling stages, cannot proceed properly which can lead to chronic wounds.[5-10] Chronic wounds are commonly caused by diabetic ulcers, prolonged inflammations, and various infections.[11-15] To address these problems, researchers aim to develop advanced wound dressing materials with anti-inflammatory and anti-infection properties, or that can deliver skin regenerating growth factors.[16-20]

Current wound dressings passively provide moist environment and temporary physical barrier to the defect site, which lacks in active tissue repair.[21, 22] To increase their bioactivity, various commercialized growth factors, such as epidermal growth factor (EGF) and fibroblast growth factor (FGF), are directly sprayed to the wound site to induce effective wound healing.[23-29] However, direct spraying method is not

practical; growth factor deposition and protection (half-life) rates are low. To improve growth factor delivery, collagen sponges are often used to transfer growth factors to the target sites.[30] Collagen sponges are soaked in growth factor dissolved phosphate-buffered saline (PBS) solution before they are applied on wounds. However, soaked collagen sponges are difficult to fixate on the wound site.[31] As an alternative, TachoSil, a commercially available adhesive collagen sponge, is used.[32] But, it is known to have side effects such as virus-based infections, hypersensitive and allergic reactions.[33] More importantly, there are no strong bonding between collagen sponges and growth factors, which leads to burst release of drugs when it is exposed to pressure. The burst release of drugs reduces bioactivity and results in secondary side effects.[34, 35] In addition, proteolytic enzymes are produced and secreted at the wound site to break down damaged extracellular matrix (ECM)[36], and growth factors are degraded by them.[37-39] This leads to rapid reduction in biological half-life of the growth factors.[40]

Complex coacervate is a liquid-liquid phase separation phenomenon that occurs when two oppositely charged polyelectrolytes, or macromolecules, are reacted to reach the net charged of 0. Since coacervates are synthesized by an electrostatic equilibrium, they are biocompatible and does not damage proteins and growth factors that are encapsulated within them.[41] Previously, coacervate was successfully designed to deliver bone morphogenetic protein 2 (BMP-2)

and Interleukin 2 (IL-2) for bone repair and T cell receptor-engineered T cell therapy, respectively.[42, 43] Fucoidan, a FDA approved natural glycosaminoglycan, was used as a anionic polymer and poly-*l*-ysine (PLL), a commercially used food preservative, was used as a cationic counterpart to fabricate the coaceravate microcapsules. Both the growth factor and cytokine were simply encapsulated during the one-pot synthesis of fucoidan/PLL coacervate. Specifically, the BMP-2 encapsulated coacervate was easily coated on the walls of collagen sponge homogeneously, since coacervates are known to have low surface tension. The coacervate coated collagen sponge was able to sustain release BMP-2 for more than 60 days, and it formed new bones precisely within the defect site without any traces of inflammations and ectopic bone formation.

In this study, adhesive fucoidan/PLL coacervate was synthesized to enhance bioactivity and introduce adhesive force to commercially available collagen sponges for wound healing. This was possible by simply functionalizing dopamine (DOPA) to fucoidan (Fig 1a). Similar to the previous studies. DOPA functionalized fucoidan (D-Fuc) was able to form coacervates with PLL. FGF2 was encapsulated into the DOPA functionalized coacervate (D-Coa) during the coacervation process (Fig 1b) with high encapsulation yield. D-Coa was able to sustain release FGF2, and protect FGF2 from collagenase and proteases. Importantly, D-Coa coated collagen sponge showed promising results through a rat

excisional wound splinting model (Fig 1c). D-Coa can be a game changing interface coating supplement for biomedical applications.

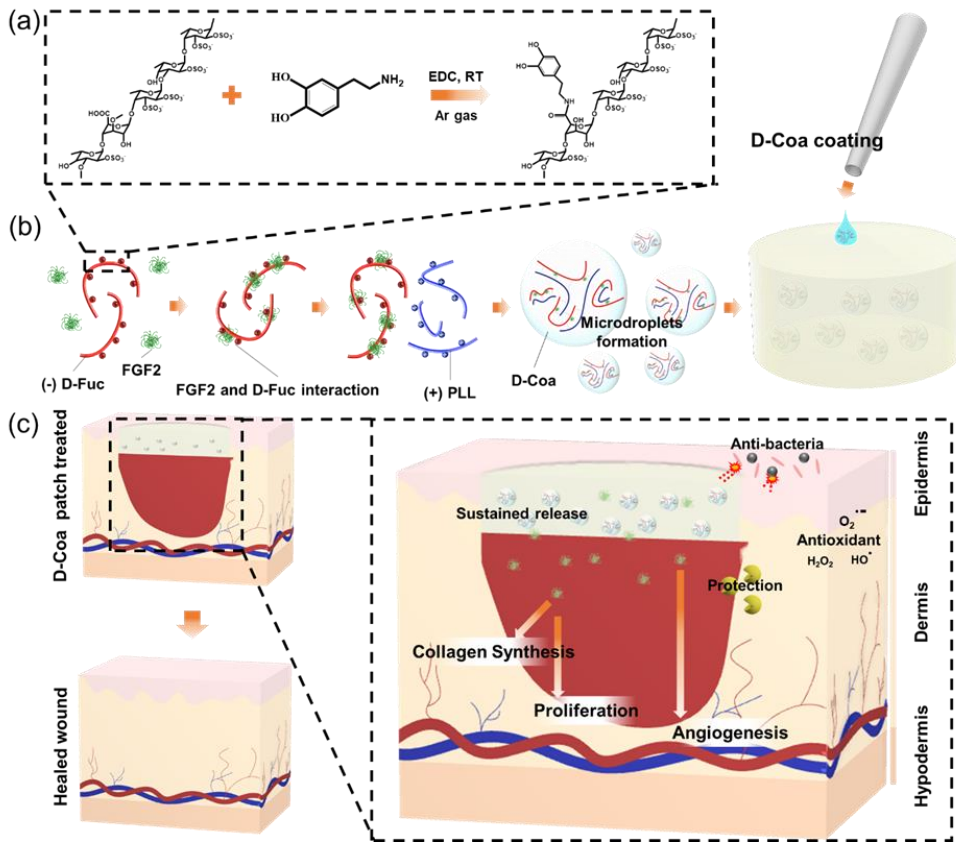

Figure 1. Schematic illustration of the dopamine-fucoidan (D-Fuc) synthesis, D-Fuc/poly-*l*-lysine (PLL) coacervate (D-Coa) formation, and wound regeneration with D-Coa coated dressing. (a-b) Preparation of D-Fuc and formation of D-Coa. (c) Wound healing mechanisms of fibroblast growth factor 2 (FGF2) containing D-Coa coated collagen sponge.

Chapter 2. Materials and methods

2.1. Materials

Fucoidan from fucus vesiculosus (purity ≥95%), poly-*l*-lysine hydrochloride (PLL; Molecular weight 15~30 kDa), dopamine hydrochloride (Dopa), hydrochloric acid 37% (HCl), n-(3-dimethylaminopropyl)-n-ethylcarbodiimide hydrochloride (EDC), deuterium oxide (D_2O), sodium hydroxide solution 30% (NaOH), sodium acetate (CH_3COONa), sodium bicarbonate ($NaHCO_3$), sodium carbonate (Na_2CO_3), albumin-fluorescein isothiocyanate conjugate (BSA-FITC), cOmplete (protease inhibitor cocktail tablets), 2-mercaptoethanol($HSCH_2CH_2OH$), methanol (CH_3OH),), phenylmethylsulfonyl fluoride (PMSF), dimethyl sulfoxide (DMSO) was purchased from Sigma-Aldrich. 1.5M Tris-HCl (pH8.8), RIPA buffer, bradford reagent, sodium dodecyl sulfate (SDS), 10X TBST with tween 20, 10X Tris glycine buffer (W/O SDS), 10X Tris glycine buffer (W/ SDS), 5X SDS-page loading buffer, TEMED, 10% Ammonium persulfate solution (APS), Iso-propyl alcohol (IPA) was purchased from Biosesang. Dulbecco's phosphate buffered saline (DPBS), dulbecco's modified eagle medium (DMEM), penicillin streptomycin (PS), fetal bovine serum (FBS), Live/Dead™ viability/cytotoxicity kit was purchased from Thermo Fisher Scientific. P44/42 MAPK rabbit mAb (1:1000), phospho-p44/42 MAPK rabbit mAb (1:2000) was purchased from Cell Signaling Technology. Human/mouse/rat beta-Actin mAb (1:5000), rabbit lgG HRP Ab (1:1000), mouse IgG HRP Ab (1:1000), Mouse/Rat FGF basic/FGF2 (Quantikine® ELISA) was purchased

from R&D Systems. Collagen type1 (10.9 mg/ml), 0.25% trypsin-EDTA was purchased from Corning. 0.1M MES buffer pH 6.0 was purchased from Tech&Innovation. Spectra/por2 dialysis membrane (MWCO = 12-14 kD) was purchased from Repligen. Fibroblast growth factor 2 (FGF2, 16.3kDa) was purchased from Pepro Tech. Collagenase type2 (290 U/mg) was purchased from Worthington. Cell count kit-8 (CCK-8) was purchased from Dojindo. 6 and 24 transwell plate (SPLInstert^{TM} Hanging) was purchased from SPL. Blotting membrane (PVDF membrane) was purchased from GVS. Precision plus protein^{TM} dual color standards was purchased from Bio-Rad. Bovine serum albumin (BSA) was purchased from Bovostar. Chemiluminescent substrate, protein quantification kit (BCA) was purchased from Biomax

2.2. Synthesis confirmation of DOPA-Fucoidan (D-Fuc)

200 mg of fucoidan and 248 mg of dopamine were dissolved in 30 ml of MES (0.1 M, pH 6.0) buffer. After completely dissolving, 410 mg of EDC was added. Thereafter, the mixture was stirred in RT for 2 h in an argon gas atmosphere. The reactant was dialyzed with a dialysis membrane (MWCO = 12-14 kD) for 3 days. Acid DI water (1 ml HCl 5 M, 1 L DI water) was used for the D-Fuc dialysis. The final product was frozen and dried, and stored in a refrigerator before use.

After DOPA conjugation on fucoidan (D-Fuc), ^{1}H NMR spectrometer (Bruker avance III 400 MHz, Bruker, USA) was performed to confirm the conjugation. D-Fuc at a concentration of 10 mg/ml was used with D_2O as a solvent. Fourier transform infrared (FTIR) spectroscopy (NICOLET is10, Thermo Scientific, USA) in the 2,000-500 cm^{-1} range was used, and 32 scans with a

resolution of 4 cm^{-1} were used. The degree of DOPA conjugation was measured using a UV-vis spectrometer (Lamda 25, PerkinElmer, USA). DI water was used as a solvent for 1 mg/ml of D-Fuc concentration. The calibration curve of DOPA was measured in a value of 280 nm with respect to 0.02-0.1 mg/ml.

2.3. Surface charge measurements on D-Coa components using Zeta potential

The surface charges of fucoidan, D-Fuc, DOPA, and poly-*l*-lysine were analyzed with a zeta potential analyzer (Zetasizer Nano ZS, Malvern, UK). Each D-Coa configuration sample was dissolved in a buffer having a different pH. The concentration of each sample was 0.1 mg/ml. The pH was prepared using 0.1 M sodium acetate for pH 3-6, 0.1 M Tris-HCl for pH 7-9, and 0.1 M sodium bicarbonate and sodium carbonate for pH 10-11.

2.4. Preparation of D-Fuc/PLL complex coacervate

D-Coa and PLL were dissolved in phosphate buffered saline pH 7.4 (PBS). Coacervate was formed at different weight ratios. To confirm the maximum turbidity of the coavervate formation, D-Fuc and PLL were dissolved at 6.25 mg/ml, respectively, and mixed at different ratios. OD value of 600 nm wavelength was measured using microplate reader (versaMax, Molecular Devices, USA). The turbidity measurement was performed immediately after coacervate formation. Time-dependent morphological changes of D-Coa were captured by optical microscope (DMIL LED, Leica, Germany).

In the case of D-Fuc, since it formed coacervate by itself, the pH was adjusted. Turbidity and optical microscope images were analyzed for pH 7, 8, and 8.5 using D-Fuc. All D-Fuc were used by

adjusting to pH 8.5−9.

2.5. Adhesive force test

Fucoidan, D−Fuc, and poly−*l*−lysine were dissolved in PBS at concentrations of 12.5, 25, and 50 mg/ml, respectively. Coacervate was then prepared at a mixing ratio of fucoidan:PLL 70:30 (wt. %) and D−Fuc:PLL 80:20 (wt. %). Each samples were centrifuged at 12,000 rpm, 4 ℃, and 10 min to settle. The supernatant was removed and applied to 10 x 10 x 1 mm^3 of pig skin (Apures, Korea). The experiment was conducted according to the Tensile strength of adhesives test (ASTM F2258), and the tool 25 x 25 mm^2 was customized and measured by attaching pig skin. The measurement conditions were 1 kN load cell at a speed of 100 mm/min. The adhesive strength was calculated using the following equation:

Adhesive strength = F/A

Where F and A are the force at the point of dividing the maximum force by the contact area.

Oil and debris on the surface of pig skin were removed before the evaluation. It was washed with pH 12−14 DI water for 15 min. Then, washed with DI water for 5 min (x 5). Remaining water was removed from the surface and dried at RT for 3~4 h before the use.

2.6. Preparation of D−Coa coated collagen sponge

Homogeneously and rapidly D−Coa coated collagen sponge (TERUPLUG, Olympus terumo biomaterials, Japan) was evaluated using confocal laser scanning microscope (Leica TCS STTED CW,

Leica Camera AG, Germany). The collagen sponge diameter of 8 mm and a thickness of 1.5 mm were used. 5 ug BSA was wetted with a sponge and coated with a sponge with 5 ug BSA loaded D-Coa. The protein yield test was performed, and the coating stabilization time was given through incubation at RT for 1, 3, and 5 min, respectively. To collect uncoated BSA, coated collagen sponge as washed twice with 100 μl PBS and measured with the fluorescence value at λ_{ex}=480 nm and λ_{em}=530 nm with microplate reader. The coating yield of free BSA-FITC and laden D-Coa was calculated using following equation:

$$\text{Protein coating yield} = (W_{total} - W_{wash})/W_{total} \times 100$$

Where W_{total} and W_{wash} indicates the weight of the total BSA-FITC and of the washed solution, respectively. D-Coa coated collagen sponge morphology were observed with top, bottom, and 3D images using a confocal laser scanning microscopy with λ_{ex}=480 nm and λ_{em}=530 nm.

2.7. Protein encapsulation evaluation

The maximum formation of coacervate was performed using a weight ratio of D-Fuc:PLL 80:20 (wt.%), and loading efficiency was compared with a weight ratio of D-Fuc:PLL 50:50 (wt.%) in consideration of the loaded protein.

The encapsulation efficiency was evaluated by mixing orders: mixing protein solution to PLL solution, followed by mixing the mixture with the D-Fuc solution (Method 1), mixing protein solution to D-Fuc solution, followed by mixing the mixture with the PLL solution (Method 2). Total concentration of D-Fuc and PLL

was fixed at 12.5 mg/ml, and concentration of model protein (BSA-FITC) was 25 ug/ml. After encapsulation, the D-Coa mixtures with BSA-FITC were centrifuged at 12,000 rpm for 10 min at RT. Each supernatant was collected, and the coacervate phase of D-Coa was remained at the bottom of the tube. The amount of unloaded BSA-FITC was analyzed by a microplate reader with fluorescence intensity in λ_{ex}=480 nm and λ_{em}=530 nm. It was quantified using the protein encapsulation yield equation.

Similarly, the encapsulation rate was evaluated for the target protein FGF2. The above-described mixing ratio (D-Fuc:PLL 80:20 (wt.%)) and method 2 were performed for FGF2 encapsulation. After FGF2 was loaded with D-Coa, the mixture was centrifuged at 12,000 rpm for 10 min at RT. The amount of unloaded FGF2 was analyzed using the FGF2 Elisa kit according to the manufacturer's protocol using a supernatant. It was quantified using the protein encapsulation yield equation.

To analyze the encapsulation rate for various concentrations, the encapsulation efficiency of various model protein (BSA-FITC) concentrations (25, 50, 100, and 200 ug/ml) were evaluated by Method 2 and weight ratio of D-Fuc:PLL 50:50 (wt.%). Each sample was processed through centrifuge and a sensing process. The supernatant was analyzed with microplate reader with λ_{ex}=480 nm and λ_{em}=530 nm for fluorescence intensity. It was quantified using the protein encapsulation yield equation. Also, it was evaluated with target protein (FGF2) with various concentrations of FGF2 (25, 50, 100, and 200 ug/ml) using FGF2 Elisa kit using protein encapsulation yield equation.

To analyze the drug encapsulation rate according to the concentration of the components that consist of the drug carrier

(D-Coa), the final D-Fuc and PLL concentrations of 12.5, 25, and 50 mg/ml were evaluated by Method 2 with weight ratio of D-Fuc:PLL 80:20 (wt.%). The model protein (BSA) concentration was 25 ug/ml. Each sample was processed through centrifuge and a sensing process. The supernatant was analyzed with microplate reader with λ_{ex}=480 nm and λ_{em}=530 nm for fluorescence intensity. The protein encapsulation efficiency was calculated using the following equation:

$$\text{Protein encapsulation yield} = (W_{total} - W_{supernatant})/W_{total} \times 100$$

Where W_{total} and $W_{supernatant}$ indicates the weight of the total model protein (BSA) or target protein (FGF2) and of the supernatant solution, respectively.

2.8. Protein releasing profile

FGF2 protein release profile of D-Coa coated collagen sponge was quantified using Method 2 and weight ratio of D-Fuc:PLL 80:20 (wt.%) by Elisa kit. 1.25 ug and 2.5 ug of FGF2 were loaded in D-Coa. The D-Coa consisted of 12.5 mg/ml of D-Fuc and PLL. The mixture was coated onto a collagen sponge and gave a coating stabilization time of 5 min at RT. After coating stabilization, incubation was performed at 37°C by immersing in 200 μl of PBS. To measure the amount of FGF2 released for 1, 3, 5, 10, 20, 30, and 60 day points, it was centrifuged in 12,000 rpm for 1min at 37°C, and the supernatant was collected and measured using an Elisa kit. After collection of supernatants, 200 μl of PBS was newly added, and the incubation was continuously performed at 37 °C. The release profile of the target protein (FGF2) was measured

using the aforementioned equation.

2.9. Protection test

The encapsulated protein protection ability of D-Coa from proteases was evaluated using collagen hydrogel and collagenase. 50ul of free BSA-FITC and BSA-FITC loaded on D-Coa was added to 50ul of collagen pre-hydrogel solution, and the final concentration of 25ug/ml BSA-FITC and 3 mg/ml collagen (collagen type 1, 10.9 mg/ml) was neutralized by adding 1N NaOH and 10X DPBS. The mixture containing free BSA-FITC and D-Coa loaded with BSA-FITC was incubated at 37 °C for 1 h and gelled. 100 U/ml collagenases II (290 U/mg) was added to 100 μl of collagen gel sample and incubated for 16 h, and each sample was collected and visualized with fluorescence and bright-field images (Leica TCS STED CW, Leica, Germany).

2.10. Biocompatibility test

In vitro cytotoxicity test was conducted based on ISO 10993-5 using the mouse embryonic fibroblasts NIH-3T3 cell line (Korea Cell Line Bank, Korea)). NIH-3T3 cell was maintained in Dulbecco's Modified Eagle's Media (DMEM) with 10 % (v/v) fetal bovine serum (FBS) and 1 % (v/v) penicillin-streptomycin (PS). The cell was cultured in humidified incubator containing 5 % CO_2 and 95 % air at 37 °C. The cell was initially seeded at 1 x 10^3 cells per well in 96-well plate (SPL) and maintained for 1 day at 37 °C under 5 % CO_2. Then, the DMEM media was replaced to fresh DMEM with D-Coa extracts. The sample was cultured for 1, 3, and 5 days at 37 °C and 5 % CO_2. After The cell viability was quantitatively determined by measuring the absorbance at 450 nm

after treatment of a CCK-8 reagent with microplate reader. The cell viability rate was also confirmed by live/dead staining kit. At each time point, calcein acetoxymethyl (Calcein AM) and ethidium homodimer-1 (EthD-1) was treated and incubated for 30 min at 37 °C. The stained sample was observed using a confocal laser scanning microscope (Leica TCS STED CW).

2.11. Proliferation test

The cell proliferation was evaluated to confirm the effect FGF2 release rate from D-Coa. NIH-3T3 cell was maintained in DMEM with 10 % (v/v) FBS and 1 % (v/v) PS. The cell was cultured in humidified incubator containing 5 % CO_2 and 95 % air at 37 °C. The cell was initially seeded at 0.5×10^4 cells per well in 24-well plate (SPLInstert™ Hanging, Korea) and maintained for 1 day at 37 °C under 5 % CO_2. Then the DMEM media was replaced with fresh DMEM. Each sample was placed on the 24-transwell. Neat collagen sponge was used as a control group, and D-Coa (D-Fuc and PLL final concentrationsof 12.5 mg/ml) with various FGF2 concentrations (0, 25, 50, 100, and 200 ug/ml) were loaded using the aforementioned mixing ratio and methods. After incubation for 1, 3, and 5 day at 37 °C under 5 % CO_2, the proliferation was quantitatively determined by a microplate reader at an absorbance of 450 nm after treatment of a CCK-8 reagent.

2.12. Bioactivity evaluation

NIH-3T3 cell was maintained in DMEM with 10 % (v/v) FBS and 1 % (v/v) PS. The cell was cultured in humidified incubator containing 5 % CO_2 and 95 % air at 37 °C. The cell was initially seeded at 2×10^5, 1×10^5, 2.5×10^4 cells per well in 6-well plate

(SPLInstert^{TM} Hanging, Korea) for 1, 3, and 5 day, respectively. After maintained for 1 day at 37 °C under 5 % CO_2, the DMEM media was replaced with fresh DMEM. Each sample was placed on a 6-transwell. Neat collagen sponge, free (FGF2 (200 ug/ml) soaked collagen sponge), and D-Coa (D-Fuc and PLL final concentrationsof 12.5 mg/ml) with various FGF2 concentrations (0, 25, 50, 100, and 200 ug/ml) were loaded using the aforementioned mixing ratio and methods. After incubation for 1, 3, and 5 day at 37 °C under 5 % CO_2, NIH-3T3 cell was collected to extract proteins. RIPA buffer and protease inhibitor cocktail was used to lysis the cell. The extracted protein was normalized to 10 ug/ml with SDS loading buffer, 2-mercaptoethanol, and PBS. The normalized extracted protein stock was qualitatively evaluated to confirm the activation of ERK band using western blot assay (mini-protein tetra cell 4-gel hand casting system and powerpac HC power supply, Bio-Rad, USA). The western blot was carried out by a SDS-page (stacking; 80 V 30min, running; 100 V, 90 min) and transfered to 10% acrylamide gel. Then 2 w/v% BSA was used for blocking. p44/42 MAPK Rabbit mAb (1:1000) and phospho-p44/42 MAPK Rabbit mAb (1:2000) were treated overnight, and human/mouse/rat beta-Actin mAb (1:5000) were treated for 1h and washed 5 times using a TBST buffer for 5 min. An antigen-antibody reaction was then performed on each sample using Rabbit lgG HRP Ab (1:1000) and mouse IgG HRP Ab (1:1000). It was washed 5 times for 5 min using the TBST buffer. After washing, the chemiluminescent was treated and detected the band using a detector (AmershamTM lmager 680, GE, USA).

The effectiveness of FGF2 was quantitatively evaluated using phospho(Thr202/Tyr204; Thr185/Tyr187)/Total ERK1/2 assay

whole cell lysate kit ((MSD® multi-spot assay system, MSD, USA). The MSD assay was performed based on the protocol provide by the manufacturer. Cell culture was proceeded in the same way as the conditions mentioned in western blot. After incubation for 1, 3, and 5 day at 37 °C under 5 % CO_2, NIH-3T3 cell was collected to extract proteins. Phenylmethylsulfonyl fluoride (PMSF) and dimethyl sulfoxide (DMSO) were added to the lysis buffer provided to MSD assay to perform protein extraction at 1, 3, and 5 day points. The concentration of each protein extraction stock was adjusted to 0.1 ug.ml using a protein quantification kit (BCA). The p-ERK and ERK were measured using MESO Secter S600MM (MSD, USA). The phospho/total ERK ratio was calculated by the following equation:

$$\% \text{ Phosphoprotein} = \text{Phospho signal/Total signal} \times 100$$

Where phospho signal and total signal indicates the phosphor ERK and total ERK of the protein extractions.

2.13. *In vivo* study

The animal experiments were approved by the Institutional Animal Care and Use Committee in Seoul National University Hospital (SNUH-IACUC; No.22-0070-S1A0) and animals were maintained in the facility accredited AAALAC International (#001169) in accordance with Guide for the Care and Use of Laboratory Animals 8th edition, NRC (2010).

Twenty of 6- to 8-week-old male Sprague-Dawley (SD) rats weighing 220~250g were divided into four groups; control, free, D-Coa0, and D-Coa200 groups. Excisional wound splinting model was

used to evaluate the accelerated wound healing capacity of the collagen sponges. Four 10-mm full-thickness wounds were made at the dorsum of SD rats as previously described.[44]

2.14. Histological evaluation

The skin samples were fixed with 4% paraformaldehyde overnight, dehydrated and embedded in paraffin wax. The paraffin-embedded tissue was then sectioned at a thickness of 4 μm. The sections were deparaffinized and stained with hematoxylin and eosin (H&E) and Masson's Trichrome (MT).

For immunohistochemistry (IHC), the paraffin-embedded samples were sectioned and placed on slides. The slides were deparaffinized and incubated with primary antibodies [PCNA (Abcam, Boston, MA, USA); CD31 (GeneTex, Irvine, CA, USA); αSMA (GeneTex); Collagen 1A1 (Santa Cruz Biotechnology, Dallas, TX, USA); and Collagen 3A1 (Santa Cruz Biotechnology)] and a secondary antibody (Invitrogen), followed by counterstained using Hematoxylin. Semi-quantitative analysis of IHC was performed using ImageJ software in two fields per section in 5 subjects per group to examine the expression of PCNA, CD31, αSMA, Collagen 1A1 and 3A1. All images should be digitized and stored in 640 × 480 or 1280 x 960 pixels resolution (original magnification x 400 and x 20, respectively).

2.15. Quantitative reverse transcription PCR (qRT-PCR)

Total RNA was isolated from the rat skin tissue using TRIzol (Invitrogen). The extracted RNA was reverse transcribed into Cdna using ReverTra Ace™ Qpcr RT Master Mix (Toyobo, Osaka, Japan). Polymerase chain reaction was conducted using SYBR Green PCR

Master Mix (Toyobo) with QuantStudio 5 (Applied Biosystems, Foster City, CA). The sequences of the primers used were as follows; COL1A1, 5’-AGGGAACAACTGATGGTGCTACTG-3’ (forward) and 5’-GGACTGCTGTGCCAAAATAAGAGA-3’ (reverse)[45]; COL3A1, 5’-AGGGAACAACTGATGGTGCTACTG-3’ (forward) and 5’-GGACTGCTGTGCCAAAATAAGAGA-3’ (reverse)[45]; MMP-2, 5’-TACAGGATCATTGGCTACACACC-3’ (forward) and 5’-GGTCACATCGCTCCAGACT-3’ (reverse)[46]; TIMP-2, 5’-TCTCGACATCGAGGACCCAT-3’ (forward) and 5’-TGGACCAGTCGAAACCCTTG-3’ (reverse)[46]; TBP-1, 5’-AAGGGAGAATCATGGACCAG-3’ (forward) and 5’- CCGTAAGGCATCATTGGACT-3’ (reverse). Results were calculated by the comparative CT method relative to an internal control reference gene (TBP-1).

2.16. Statistical analysis

Comparison between four groups was performed using one-way ANOVA followed by a Tukey post hoc analysis. All results were analyzed and graphed using GraphPad Prism 8.0 (GraphPad Software, La Jolla, CA) and IBM SPSS Version 22 (IBM Corp., Armonk, NY, USA). Differences were considered statistical significant when $P < 0.05$. * denotes $P < 0.05$, ** denotes $P < 0.01$, *** denotes $P < 0.001$, and **** denotes $P < 0.0001$.

Chapter 3. Results and discussions

3.1. Preparation and characterization of DOPA conjugated fucoidan (D-Fuc)

Previous studies were able confirm that coacervate of fucoidan and PLL was a promising drug delivery vehicle for BMP-2 and Il-2. It had high encapsulation efficiency, prolonged sustain release profile, and high protection ability from proteolytic enzymes.[42, 43] However, it lacked adhesive force for a robust fixation on defects. To introduce adhesiveness, complex coacervate was fabricated using DOPA functionalized fucoidan since DOPA is an underwater adhesive agent.[41, 47-60]

As DOPA is known to be insoluble in water when it is oxidized. DOPA functionalization on fucoidan was conducted in different pHs in deionized water. As shown in Fig S1a, DOPA conjugation was not possible at pH 1.5 while it was possible in higher pHs (pH 3~6). Although functionalized DOPA was confirmed through both fourier transform infrared (FTIR) and UV-vis spectroscopies (Fig S1b & c), D-Fuc was insoluble in water due to the oxidation of DOPA. Therefore, DOPA conjugation was performed in pH 6 2-morpholin-4-4ylethanesulfonic acid (MES) buffer. As shown in Fig 1, DOPA was successfully conjugated with fucoidan. DOPA peaks at 6.9~7.6 ppm and representative fucoidan peaks were both observed through a nuclear magnetic resonance (^{1}H-NMR) spectroscopy (Fig 2a). FTIR spectroscopy confirmed 1550 cm^{-1} (amide II band, N-H bending) and 1650 cm^{-1} (amide I band, C=O stretching) peaks, which represent DOPA (Fig 2b). As shown in Fig 2c, UV-vis

spectrometer also confirmed the presence of DOPA (280nm peak). DOPA content within D-Fuc was quantified by comparing the DOPA concentration calibration curve (Fig S2) to the UV-vis measured DOPA concentration, which was 9-15 wt. %.[53]

Complex coacervation occurs between oppositely charged polyelectrolytes via electrostatic interaction. Therefore, the anionic and cationic polyelectrolytes should retain their surface charge during the coacervation process. Since biomedical applications are required to perform in physiological condition, coacervation should occur and maintain as coacervates at pH 7.4. To confirm surface charges of D-Fuc and PLL, zeta potential analyzer was used and measurements were compared in pH ranging from 3 to 11. As shown in Fig 1d, D-Fuc and PLL had opposite surface charges from pH 3 to 9, which was similar to the previous study.[42] Although DOPA was shown to have negative surface charge in pH 7 to 9, DOPA conjugation did not affect D-Fuc surface charge significantly. D-Fuc/PLL coacervation was possible in the physiological condition of pH 7.4.

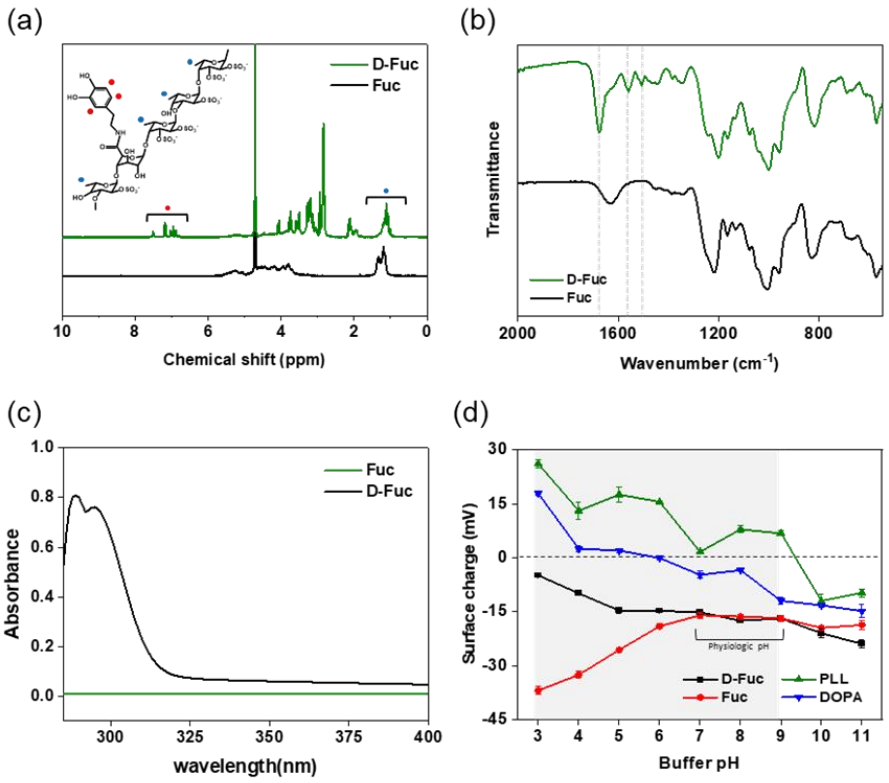

Figure 2. Dopa functionalized fucoidan confirmation. (a) ^{1}H−NMR spectrum of fucoidan (Fuc) and D−Fuc. (b) FTIR spectrum of Fuc and D−Fuc. (c) UV−vis spectrum of Fuc and D−Fuc. (d) Isoelectric points of Fuc, D−Fuc, DOPA, and PLL by surface charge measurements (n=3). pH 3−9, the background, indicates the range in which the net charges can be neutralized.

3.2. Preparation and confirmation of adhesive D−Fuc/poly−*l*−lysine coacervate (D−Coa)

Coacervation of D−Fuc/PLL coacervate (D−Coa) was confirmed through turbidity measurements and micro−droplet visualization using optical microscope. Interestingly, during the process of dissolving D−Fuc and PLL in PBS, turbidity and micro−droplets were detected in D−Fuc solution (Fig S3). As shown in Fig S3a, self−coacervation of D−Fuc was observed in pH 3. This was

possibly due to DOPA inducing hydrogen bonding, pi-pi interaction, and DOPA-DOPA interaction.[61-64] However, when pH was adjusted to pH 8.5 or higher, no micro-droplets were detected. From the turbidity measurements in Fig S3b, it was confirmed that the turbidity was not increasing as the concentration of D-Fuc increased at pH 8.5. Therefore, pH adjustment to pH 8.5 was required to prevent self-coacervation of D-Fuc.

As shown in Fig 3a, turbidity was measured by various mixing ratios of D-Fuc and PLL. Among the various mixing ratios, D-Fuc:PLL = 80:20 (wt. %) showed the highest turbidity, which represents the maximum D-Coa formation yield. D-Fuc and PLL solutions were transparent before the coacervation process. When the two polyelectrolytes were mixed together, it spontaneously formed opaque micro-droplets, or coacervates (Fig 3b). Similar to the previous study, aggregation of micro-droplets were observed as time passed.[42, 43] Aggregation phenomenon occurs when oppositely charged polyelectrolytes experiences electrostatic equilibrium; separating water molecules. This leads to increase in hydrophobicity of the coacervate surface. Then, hydrophobic-hydrophobic interactions further forms bulk coacervates.[41] On the contrary, when the surface charges of the polyelectrolytes become similar, repulsive force is formed between them; resulting in dissociation of the coacervate. Therefore, reversible dissociation and reformation through pH adjustment is possible.[65] The reversibility of D-Coa was evaluated by changing pH. As shown in Fig S4, pH after the coacervation between D-Fuc and PLL was pH 7~8. When NaOH was introduced to increase pH (pH 12), D-Coa dissociated spontaneously. To reform coacervates, HCl was added to reduce pH down to pH 8~9, and D-Coa was detected. This

suggested that programmed drug release from D-Coa is possible by modulating pH.

The adhesive force of D-Coa was confirmed by adhesion strength test using pig skin as a testing substrate (supplementary video). D-Coa with different polyelectrolyte concentrations (12.5, 25, and 50 mg/ml) were compared to fucoidan/PLL coacervate (Coa, coacervate without DOPA conjugation). As shown in Fig 3c, all the concentrations have shown significantly higher adhesive strength for D-Coa. Specifically, Coa displayed 27.71 ± 14.36, 36.75 ± 13.88, and 34.21 ± 32.4 kPa for polyelectrolyte concentrations of 12.5, 25, and 50 mg/ml, respectively. While D-Coa had adhesive forces of 213.83 ± 28.45, 330.2 ± 51.15, and 332.38 ± 60.62 kPa, for polyelectrolyte concentrations of 12.5, 25, and 50 mg/ml, respectively. Adhesive force of D-Coa was at least 7.7 fold higher than that of the Coa. This was due to DOPA having mfp-3 and mfp-5 proteins, which provide strong underwater adhesion.[54]
The adhesive ability of D-Coa was further evaluated by cyclic loading, or multiple attachment-detachment repeating cycles, test. The polyelectrolyte concentration of 12.5 mg/ml was applied to pig skin substrate. As shown in Fig 3d, average adhesive strength was 183 kPa, and it tended to increase as the repeated cycles were increasing. This was possibly due to evaporation of water molecules between D-Coa, which allows stronger adhesive force by D-Coa microcapsules aggregating to a bulk conformation. D-Coa was also shown to adhere strongly on various materials, such as metal, nitrile, and polypropylene (Fig S5).

To investigate the coating ability of D-Coa, surface morphology, and coating yields were evaluated by dropping D-Coa solution onto a collagen sponge. BSA-FITC was encapsulated in D-Coa,

following the previous study.[42] After 1, 3, and 5 min of dropping D-Coa solution onto a collagen sponge, collagen sponges were visualized with fluorescence imaging. As shown in Fig 3e, top and bottom surfaces of the sponge were homogeneously coated. Specifically, coating yield of D-Coa was higher than Coa, regardless of the coating time and polyelectrolyte concentrations (Fig 3f). All the D-Coa coating yields were above 83 %, while highest Coa coating was 77.57 ± 4.95 %. This was possibly due to the adhesive force of DOPA enhancing coating ability. The rapid and homogeneous coating ability of D-Coa can allow effective bioactive coatings with various proteins and drugs.

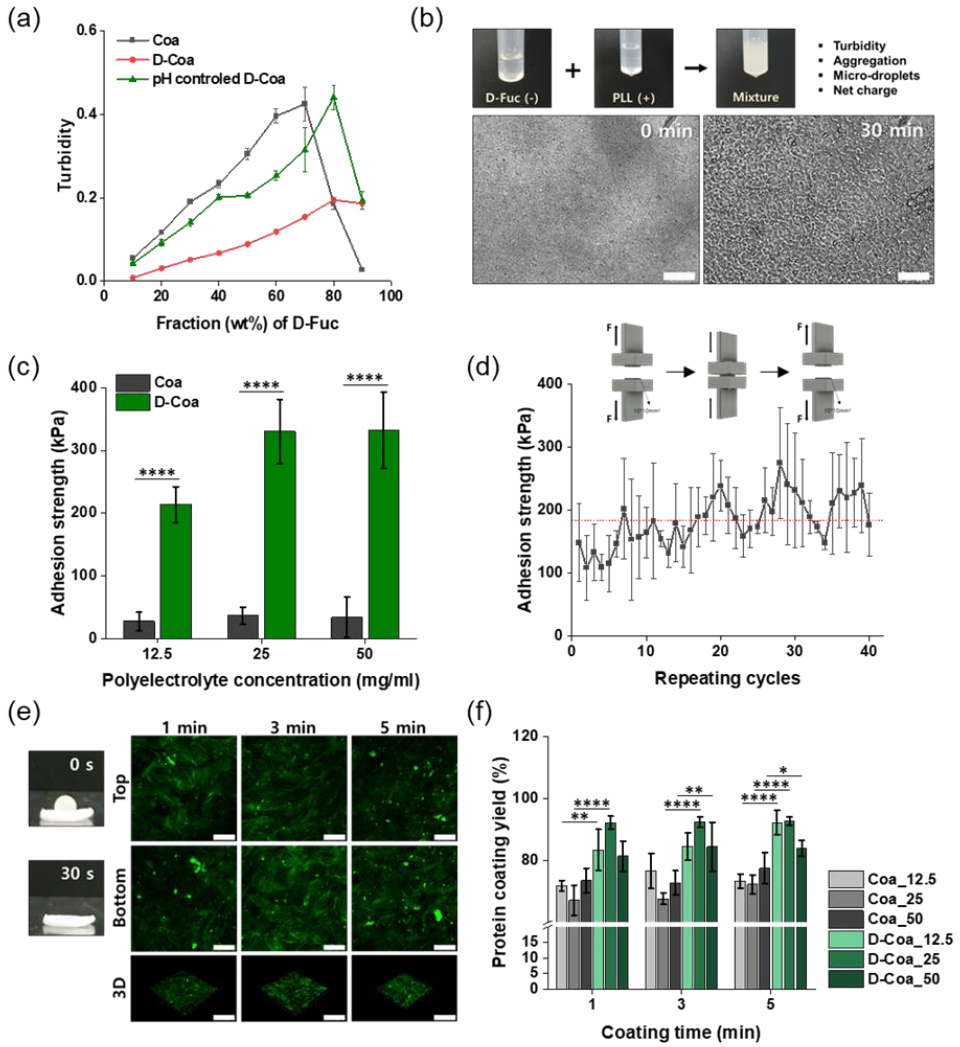

Figure 3. Coacervation between D-Fuc and PLL. Adhesive force and coating abilities of D-Coa. (a) Turbidity measurements of Coa (n=5), D-Coa (n=2), and pH-controlled D-Coa (n=5) suspensions at different polyelectrolyte mixing ratios. (b) Representative images of the D-Coa coacervation processes in PBS (pH 7.4). Optical microscopic images of D-Coa instantly after and 30 min after the coacervation process. Scale bar = 20 μm. (c) Adhesive strength of Coa (n=3) and D-Coa (n=5) with different polyelectrolyte concentrations (12.5, 25, and 50 mg/ml). Pig skin was used as a testing substrate. D-Coa was fabricated with D-

Fuc:PLL ratio of 80:20 (wt. %). (d) Cyclic adhesive strength measurements of D-Coa. The polyelectrolyte concentrations was 12.5 mg/ml (n=3). Pig skin was used as a testing substrate. D-Coa was fabricated with D-Fuc:PLL ratio of 80:20 (wt. %). (e) Representative photographs of D-Coa coating on a collagen sponge within < 30 s (left). Fluorescence images of D-Coa coated collagen sponge with different coating stabilization times (top, bottom, and 3D images). BSA-FITC was encapsulated within D-Coa. Scale bar = 100 μm. (f) Coating yields of Coa and D-Coa with different polyelectrolyte concentrations (12.5, 25, and 50 mg/ml) (n=5) and coating stabilization times (1, 3, and 5 min). All values are expressed in mean ± SD. The statistical analysis was evaluated using one-way analysis of variance (ANOVA) with Tukey's multiple comparison test. Statistical significance is specified as $p^{*} < 0.05$, $p^{**} < 0.01$, and $p^{****} < 0.00001$.

3.3. D-Coa as a drug delivery coating system

To confirm D-Coa's ability as a drug delivery vehicle[36], protein encapsulation efficiency[39, 66-68], protein release profile, and protection against proteolytic enzymes were systematically evaluated.[37, 38, 40] As shown in Fig S6, the authors hypothesized that the sulfate groups from fucoidan can interact with arginine, lysine, and histidine domains from proteins, which can induce high binding affinity. BSA-FITC was used as a model protein to investigate encapsulating ability of D-Coa. As shown in Fig 4a & b, protein mixing orders and mixing ratios were compared. Mixing orders were varied by introducing the model protein to PLL (method 1) or D-Fuc (method 2) first. Then, two different mixing ratios; D-Fuc:PLL ratios of 80:20 and 50:50 (wt. %), were

compared. Final BSA-FITC concentration was 25 ug/ml. Encapsulation yield of the model protein was above 80 %, regardless of the different parameters. There was no significant difference in mixing orders, however, mixing ratios of 50:50 was shown to have a higher encapsulating yield (93.76 ± 1.19 %). Furthermore, to evaluate the effect of BSA-FITC and D-Coa consisting polyelectrolytes concentrations on the encapsulation efficiency, method 2 with 50:50 (wt. %) mixing ratio was used. As shown in Fig 3c, highest encapsulation rate of 94.72 ± 1.17 % was observed for the lowest BSA-FITC concentration (25 ug/ml), while encapsulation rates were similar for higher BSA-FITC content. Similar trend was observed for varying polyelectrolyte concentration; 94.72 ± 1.17, 82.88 ± 1.51, and 82.08 ± 5.57 % for 12.5, 25, and 50 mg/ml, respectively (Fig 3d). The authors would like to point out that the decrease in the encapsulation efficiency rate as the polyelectrolyte concentration increase was due to the loss of D-Coa. Higher D-Coa concentration was more prone to adhering on the surface of Eppendorf tubes and pipette tips. Therefore, 12.5 mg/ml concentration was used for the rest of the experiments.

After confirming the encapsulation ability of D-Coa using a model protein, FGF2 was encapsulated in D-Coa. Different to the BSA-FITC encapsulation, there was no significant difference in encapsulation yield for varying mixing order and mixing ratios (Fig 4e). The encapsulation yield was more than 93 % for all the methods. Furthermore, to evaluate the effect of FGF2 concentration on the loading yield, 25, 50, 100, and 200 ug/ml of FGF2 was encapsulated to D-Coa of method 2 with 80:20 (wt. %). As shown in Fig 4f, there was no difference in encapsulation yield. All the

yield rates were more than 96 %, which was higher than that of the BSA-FITC encapsulation.

To evaluate FGF2 release profile from D-Coa coated collagen sponge, FGF2 with 100 and 200 ug/ml concentrations were encapsulated in D-Coa, and 5 min of coating stabilization time was used. Then, the coated collagen sponge was immersed in PBS at 37 ºC and incubated for 60 days. As shown in Fig 4g, sustained release of FGF2 was observed for 60 days of incubation after an initial burst release, which was also observed in Coa with BMP-2 and IL-2 encapsulation in previous studies[42, 43]. Cumulative release was 8.98 ± 0.03 and 8.22 ± 0.18%, for 100 and 200 ug/ml concentrations respectively. As a further investigation, effect of DOPA on release profile was conducted. BSA-FITC encapsulated Coa coating with 5 min of coating stabilization time was used, and the coated collagen sponge was incubated for 30 days. As shown in Fig S7, cumulative release rate of 106.72 ± 4.48, 69.11 ± 6.03, and 65.23 ± 7.73 % for 12.5, 25, and 50 mg/ml polyelectrolyte concentrations were observed, respectively. This were higher release rates than both the D-Coa and Coa from the previous study[42], since coating stabilization time of 120 min was used previously. DOPA conjugation was able to shorten the coating stabilization time by 24 fold, due to its adhesiveness.

The high encapsulation yields of BSA-FITC and FGF2 was possibly from their interaction with D-Fuc. As previously mentioned in Fig S6, proteins can interact with sulfate groups from fucoidan and aromatic rings from DOPA. Aromatic rings from proteins can form pi-pi and pi-cation interactions with DOPA.[69, 70] There are abundant electrostatic domains and aromatic rings from BSA-FITC and FGF2, which allow high binding affinity towards D-

Fuc and high encapsulation yield within D-Coa (Fig S8).

Protection ability of D-Coa against proteolytic enzymes was evaluated following the previous study.[42] In short, BSA-FITC and BSA-FITC encapsulated D-Coa were embedded in collagen hydrogel, then the mixtures were incubated with collagenase II for 16 hr. The amount of BSA-FITC in the lysates after collagenase treatment was visualized through fluorescence spectrometer and bright field microscopy. As shown in Fig 4h, hardly any BSA-FITC was detected for unprotected BSA-FITC loaded collagen hydrogel since collagenase degraded all the proteins. On the other hand, BSA-FITC was confirmed in D-Coa embedded hydrogel (Fig 4i). Similar to Coa, D-Coa was able to protect encapsulated protein from proteolytic enzymes. The high encapsulation yield and effective protection ability of D-Coa on proteins can prolong half-life and bioactivity of growth factors.

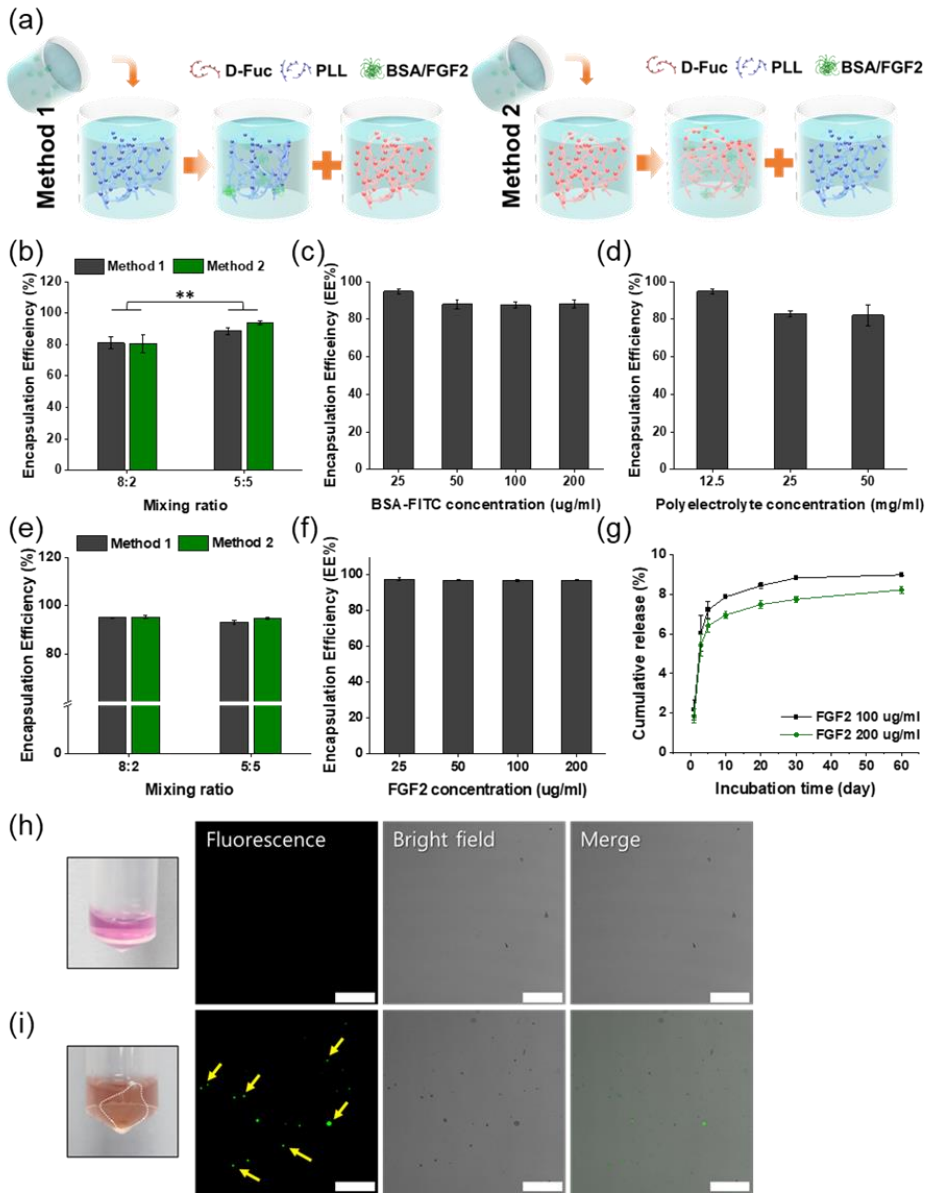

Figure 4. Protein encapsulation efficiency, releasing profile, and protection ability of D-Coa. (a) Schematic illustrations of protein encapsulation methods within D-Coa using two different mixing orders. (b) The effects of the mixing order and weight ratio of D-Fuc and PLL (80:20 and 50:50) on BSA-FITC encapsulation yields (n=5). (c) BSA-FITC encapsulation yields at different concentrations (25, 50, 100, and 200 ug/ml). D-Coa was fabricated with Method 2 and D-Fuc:PLL weight ratio was 50:50 (wt. %)

(n=5). (d) BSA-FITC encapsulation efficiency of D-Coa at different polyelectrolyte concentrations (12.5, 25, and 50 mg/ml D-Coa was fabricated with Method 2 and D-Fuc:PLL weight ratio was 50:50 (wt. %) (n=5). (e) The effects of mixing order and weight ratio of D-fuc and PLL (80:20 and 50:50) on FGF2 encapsulation yields (n=5). (f) FGF2 encapsulation yields at different concentrations (25, 50, 100, and 200 ug/ml). D-Coa was fabricated with Method 2 and D-Fuc:PLL weight ratio was 80:20 (wt. %) (n=5). (g) In vitro release profiles of D-Coa with different FGF2 concentrations (100 and 200 ug/ml) (n=5). D-Coa was fabricated with Method 2 and D-Fuc:PLL weight ratio was 80:20 (wt. %), and coating stabilization time on collagen sponge was 5 min. (h) Unprotected BSA-FITC and (i) BSA-FITC encapsulated D-Coa embedded collagen hydrogels after 16 h of collagenase treatment. Scale bar 100 μm. D-Coa was fabricated with Method 2 and D-Fuc:PLL weight ratio was 50:50 (wt. %), and the final BSA-FITC concentration was 25 ug/ml. All values are expressed in mean ± SD. The statistical analysis was evaluated using one-way analysis of variance (ANOVA) with Tukey's multiple comparison test. Statistical significance is specified as $p^{**} < 0.01$.

3.4. *In vitro* biocompatibility and bioactivity evaluations of D-Coa coated collagen sponge

Biocompatibility of D-Coa was evaluated by indirect contact method. NIH-3T3 fibroblast cell was cultured with extracts of D-Coa for 5 days. Cell count kit (CCK)-8 and Live/Dead assays were performed to verify the cytocompatibility of D-Coa. CCK-8 assay revealed that presence of D-Coa did not affect cell viability (Fig 5a). Moreover, the proliferation and morphological elongation of

fibroblasts increased for cells cultured with D-Coa when compared to the non-treated group (Fig 5b).

To evaluate effect of D-Coa coating on cell proliferation, control (neat collagen sponge) and D-Coa coated collagen sponges with various FGF2 concentrations (0, 25, 50, 100, and 200 ug/ml) were cultured in transwell plates with NIH-3T3. As shown in Fig 5c, proliferation ratios of the D-Coa coated groups tend to decrease until 3 days of culture. The catechol group from D-Coa possibly suppressed cell proliferation in the early stage.[71] However, proliferation rates of all the samples increased after 5 days of culture. Another possibility for FGF2 encapsulated D-Coa samples is that the excessive release of FGF2 in the early stage, which was observed in Fig 4g. ED_{50} (dose required to achieve 50 % of a desired effect) of FGF2 is known to be $\leq$ 0.2 ng/ml. The burst release of FGF2 in the first 5 days of culture possibly released higher FGF2 concentration than ED_{50}, which inhibits cell proliferation.

To further confirm bioactivity of the D-Coa coating, extracellular signal-regulated kinase (ERK) activation was evaluated on control (neat collagen sponge), free (FGF2 soaked collagen sponge), and D-Coa coated collagen sponges with various FGF2 concentrations (0, 25, 50, 100, and 200 ug/ml). Since FGF2 binds to FGF receptor (FGFR) and induce downstream signaling pathways, such as ERK pathway. Specifically, FGF bound FGFR activates dimerization of cytoplasmic tyrosine kinase by phosphorylation of tyrosine residues. Then, the phosphorylated tyrosine residues serve as the docking sites for the downstream signal molecule. The downstream signaling pathways include Ras-Raf-MEK-MAPKs, and ERK [28, 72, 73]. As shown in Fig 5d & S9, all the sample groups showed

phospho-ERK (p-ERK, or activated ERK) bands, regardless of the culture period. ERK activation in the control and free groups were due to the no presence of any cytotoxic agents, and fetal bovine serum culture media inducing cell proliferation. To quantify p/total ERK ratio, meso scale discover (MSD) multi-spot assay was used (Fig 5e). There was no significant differences in the p-ERK/total ERK ratio for all the sample groups after 1 day of culture. After 3 days of culture, sample groups without FGF2 (control and D-Coa0 (D-Coa with 0 ug/ml of FGF2)) had lower p-ERK/total ERK ratio compared to that of the sample groups with FGF2. On the 5^{th} day, D-Coa50 and 100 had the highest ERK ratio, while other sample groups' ERK activity were lower or similar to the control group. Interestingly, ERK activation of D-Coa200 was lower than the control. This was possibly due to the excessive release of FGF2, which the released concentration was higher than ED_{50}. The bioactivity evaluations were able to confirm that D-Coa coating enhances prolonged release of FGF2, which induce higher cell proliferation.

Furthermore, antioxidant ability of D-Coa was evaluated, since catechol groups from DOPA is known to have antioxidant properties.[74] Antioxidant ability can be an important factor for enhancing wound healing. In wounds, various immune, and inflammatory responses occur which produce high levels of reactive oxygen species (ROS). Although mild ROS levels are known to have beneficial effects on wound healing, high levels of ROS can lead to chronic wounds.[75, 76] As shown in Fig S10, DOPA conjugated fucoidan (D-Fuc) and D-Coa was able to reduce violet color of 1,1-diphenyl-2-picryl hydrazyl (DPPH) solution to yellow colored solution. The nitrogen atom in DPPH was able to receive hydrogen

atom from DOPA. D-Coa can elevate ROS levels in wound sites to enhance wound healing and tissue regeneration.[77]

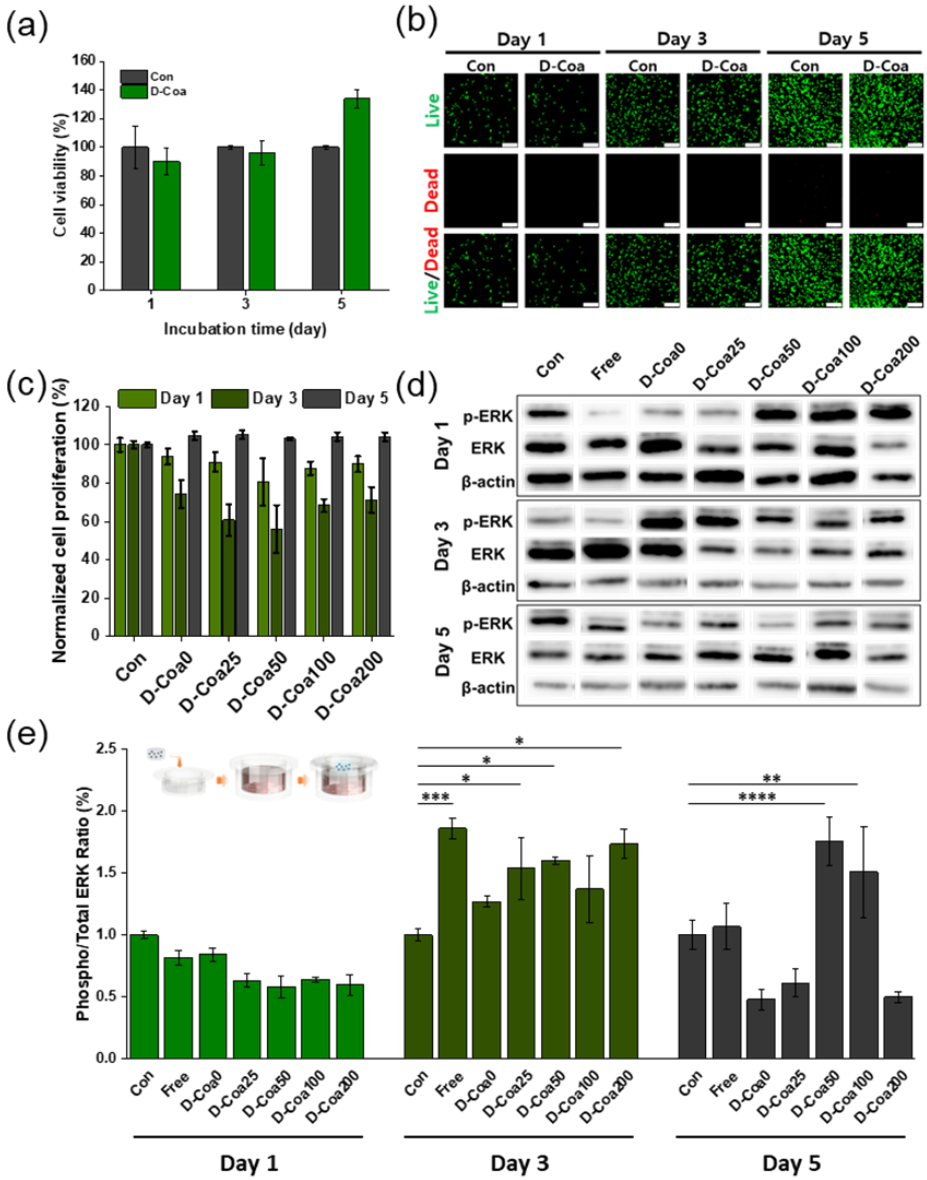

Figure 5. In vitro biocompatibility and bioactivity of D-Coa coating. (a) Quantification of cell viability test on control (non-treated cells) and D-Coa treated cells using mouse fibroblast NIH-3T3 by CCK-8 assay (n=5). (b) Fluorescent images of Live/Dead assay after 1, 3, and 5 days of culture. Live cells are stained with calcein-AM (green) while dead cells are stained with EthD-1 (red).

Scale bar = 200 μm. (c) Quantification of NIH-3T3 proliferation test on control (neat collagen), and D-Coa coated collagen sponges with various FGF2 concentrations (D-Coa0, 25, 50, 100, and 200; numbers refer to concentration of FGF2 in ug/ml) (n=4). (d) Representative western blot bands of phosphor-ERK (p-ERK) and total ERK from the cell lysate that was co-cultured with control (neat collagen), and D-Coa coated collagen sponges with various FGF2 concentrations (n=3). (e) Quantified Phospho-ERK/Total ERK ratio ($3 \leq n \leq 6$) results from the cell lysate that was co-cultured with control (neat collagen), and D-Coa coated collagen sponges with various FGF2 concentrations. D-Coa was fabricated using Method 2 with D-Fuc:PLL weight ratio of 80:20 (wt. %) All values are expressed in mean ± SD. The statistical analysis was evaluated using one-way analysis of variance (ANOVA) with Tukey's multiple comparison test. Statistical significance is specified as $p^* < 0.05$, $p^{**} < 0.01$, $p^{***} < 0.0001$, and $p^{****} < 0.00001$.

3.5. *In vivo* wound healing evaluation of D-Coa coated collagen sponge

Wound healing ability of collagen sponge with FGF2 loaded D-Coa coating was evaluated through an excisional wound splinting model on rat. In order to prevent wound closure by skin contraction, and allow wound healing through granulation and re-epithelialization, a silicone ring was placed around each full-thickness wound (diameter: 10 mm) on dorsum of rats (n=4 wounds per rat) [44]. Control (neat collagen sponge), free (FGF2 soaked collagen sponge), D-Coa0 (D-Coa coated collagen sponge), and D-Coa200 (FGF2 encapsulated D-Coa coating on collagen

sponge) groups were compared (Fig 6a). Although D-Coa200 was observed with low bioactivity in enclosed in vitro test, the authors hypothesized that the higher concentration of FGF2 was necessary for the in vivo experiment. For the D-Coa0 and 200 groups, the collagen sponges were coated with D-Coa, and FGF2 encapsulated D-Coa instantaneously after the wound surgeries were made. The collagen sponges were then placed on the splinted wounds for 2 weeks.

Representative photographs of the residual wounds in each group are shown at different time points in Fig 6b. D-Coa200 implanted group significantly promoted faster wound closure rate. Macroscopically, there were significant differences in the repaired wound area between the D-Coa200 (7.4 ± 3.9%) and other groups (36.5 ± 8.0 %, 20.5 ± 9.2 %, and 17.1 ± 5.4 % for control, free, and D-Coa0 groups, respectively.) after 2 weeks of post-surgery (Fig 6c). In a pilot study, all the wounds were mostly regenerated for all the implants after 3 weeks of post-surgery. Despite the similar macroscopic findings, subsequent histological analysis revealed notable differences in the degree of tissue regeneration for the dermal structure between D-Coa200 and other implant groups (Fig S11). Histological examinations after 2 weeks of post-surgery showed that re-epithelialization from the wound margin was followed by degradation of the collagen sponge. In addition, remodeling of dermis layer was observed with cells and new blood vessels infiltrating within D-Coa200 (Fig 6d). The re-epithelialization and remodeling of the wound was noticeably accelerated for the wound with D-Coa200 implant. The sustained release of FGF2 from D-Coa200 evidently enhanced tissue regeneration, while free group showed inferior wound healing due

to the short half-life of FGF2 and imprecise drug delivery.

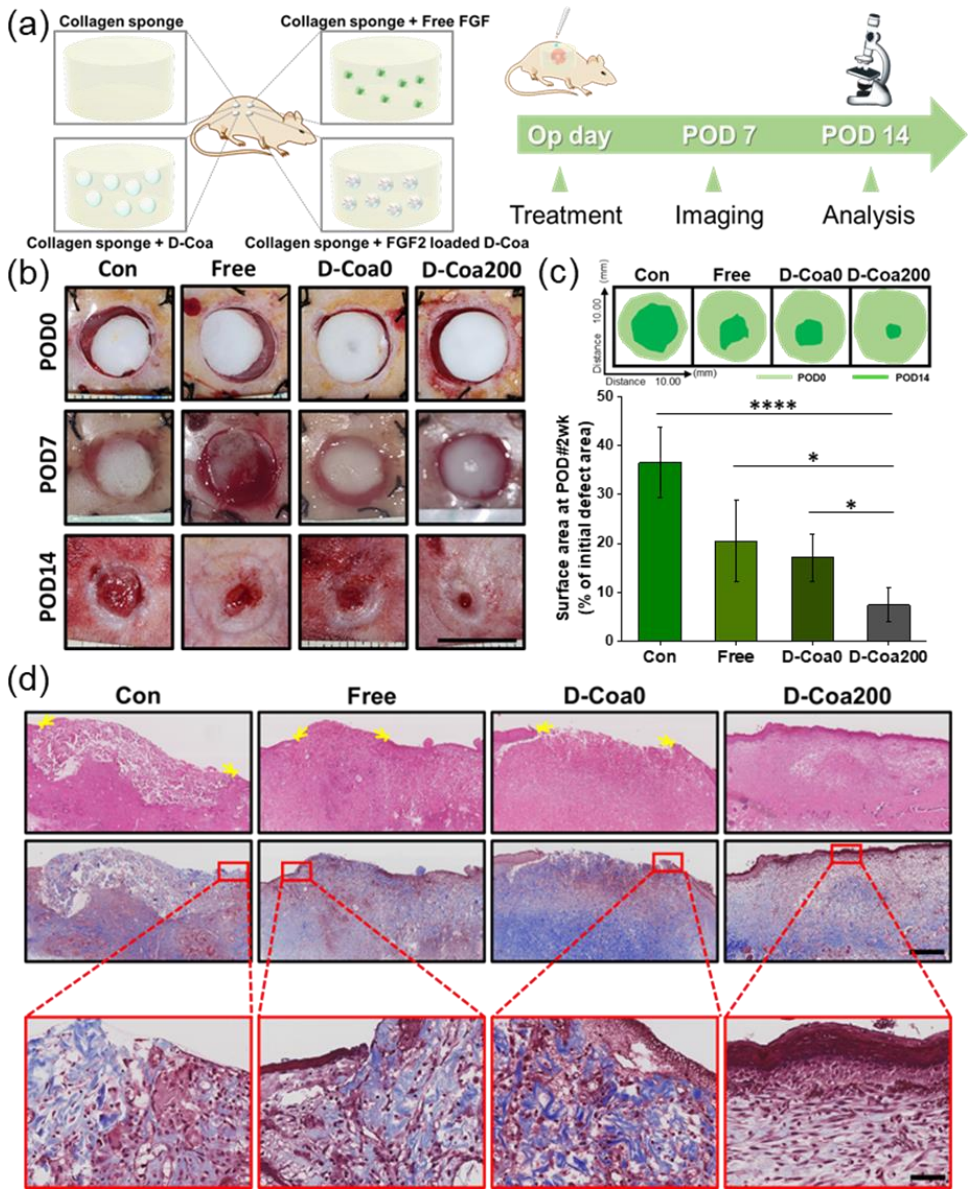

Figure 6. Effect of FGF2 encapsulated D-Coa coating on bioactivity of collagen sponge. (a) Schematic illustration of the in vivo study using a full-thickness excisional wound splinting model on rat. (b) Representative photographs of wounds with Control (neat collagen sponge), free (FGF2 soaked collagen sponge), D-Coa0 (D-Coa coated collagen sponge), and D-Coa200 (FGF2 encapsulated D-

Coa coating on collagen sponge) implants at 0, 7 and 14 postoperative day (POD). Scale bar = 1 cm. (c) Quantification of relative sizes of the residual wounds (% of the original size) at POD14 (n = 5 rats per group). (d) Representative images of Hematoxylin and Eosin (H&E) and Masson's Trichrome (MT) staining on wounds with different implants at POD14 (original magnification x 20 for the upper row, and x 400 for the lower row, respectively). Yellow arrows indicate edges of the non-epithelialized wound portions in the Con, Free and D-Coa0 implanted groups. D-Coa200 implant showed notable improvements in re-epithelialization, degradation of the collagen sponge, and dermis remodeling. Scale bars = 1 mm and 100 μm for upper and lower row, respectively.

To evaluate cell proliferation during wound healing, immunohistochemistry (IHC) for proliferating cell nuclear antigen (PCNA) was performed. The number of PCNA-positive cells in the D-Coa200 group was significantly higher than other groups (all $P<0.01$; Fig 7a & b). Similar trend was observed for expressions that represent angiogenesis and vascularization. The areas with CD31-positive newly formed with high density, and αSMA-positive mature blood vessels was also significantly higher for D-Coa200 implanted wound than wounds with other implants (Fig 7a, c, & d). These findings were consistent with previous studies, and well-known characteristics of FGF as a potent mitogen and chemoattractant for various cells (e.g. fibroblasts, endothelial cells) associated with wound healing.[78] Sustained release of FGF2 from the D-Coa coating significantly enhanced cell proliferation and vascularization.[79]

Further analyses regarding ECM deposition were performed. Masson's Trichrome staining showed that collagen deposition was significantly increased in D-Coa200 group compared to that of the other groups (all $P<0.01$; Fig 7a and e). The well-organized collagen fibers were noted in D-Coa200 implanted group. Fibroblasts are known to secrete collagen and fibronectin which are major proteins of the ECM.[80] Fibronectin is important in ECM formation by interacting with various cells and cytokines.[81] The initial fibronectin network provides a conduit for fibroblast migration, which leads to collagen type I and III network formation.[82, 83] IHC revealed that the expression of fibronectin was significantly higher in wounds with D-Coa200 (all $P<0.0001$; Fig 7a and f). In the remodeling phase, the unorganized collagen type III is degraded by proteases, then replaced by the mature collagen type I fibrils. The increase in ratio of collagen type I to type III represents higher stability of newly regenerated tissues in wounds.[84] The results of reverse transcription polymerase chain reaction (RT-PCR) indicated that D-Coa200 group had significantly higher collagen type I/III ratio compared to that of the other groups (all $P<0.001$; Fig 7g). Additionally, the dynamic remodeling of ECM is regulated by the balance of proteolytic matrix metalloproteinases (MMPs) and tissue inhibitors of metalloproteinases (TIMPs). In particular, MMP-2 is secreted by fibroblasts and inhibited by TIMP-2. The ratio of MMP-2/TIMP-2 is reported to be highly expressed in non-healing wounds.[46] Quantitative RT-PCR showed that MMP-2/TIMP-2 mRNA expression ratio was significantly lower in wounds with D-Coa200 than that in the control and free groups ($P=0.0036$; fig 7h). Overall, in vivo evaluations were able to confirm that D-Coa200 can release FGF2 in controlled manner at

an effective dose within the wound site.

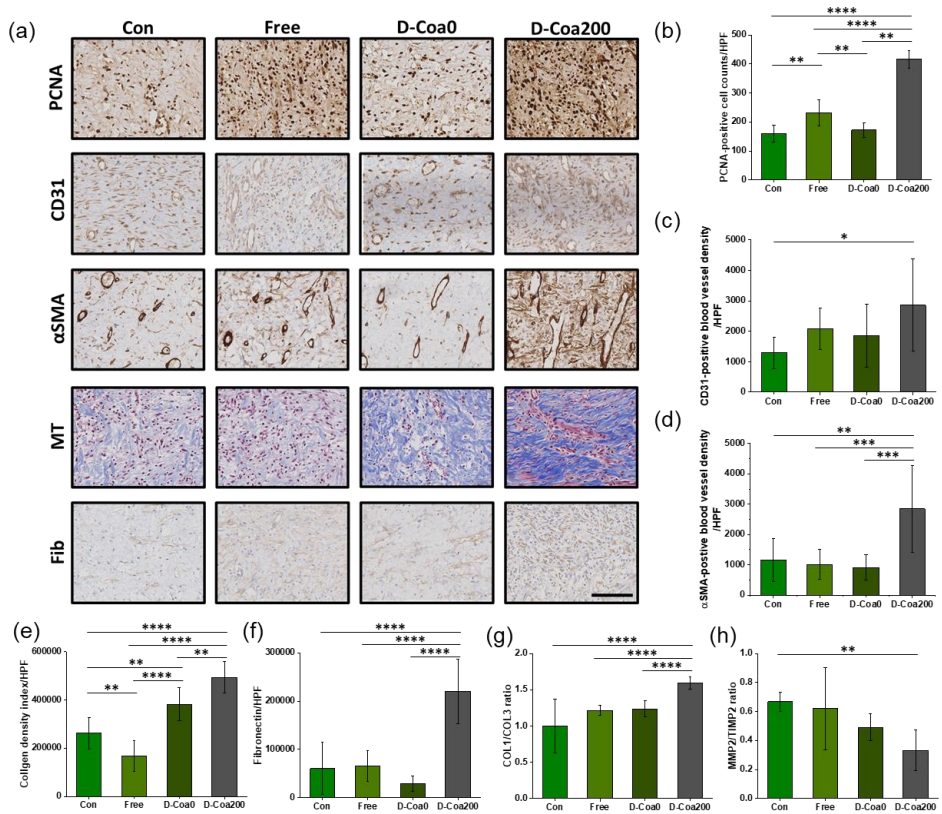

Figure 7. Enhanced cell proliferation, angiogenesis, collagen deposition, and tissue regeneration through FGF2 encapsulated D-Coa coating. (a) Representative immunohistochemistry (IHC) and MT stained high power field images of wounds with different implants (magnification x 200). Scale bar = 100 μm. Quantitative analysis of (b) proliferating cell nuclear antigen (PCNA) cell proliferation marker, (c) CD31-positive density of newly-formed blood vessels, (d) α-smooth muscle actin (α-SMA) marker of mature blood vessels, (e) collagen fiber density, (f) fibronectin, (g) reverse transcription-polymerase chain reaction (qRT-PCR) of collagen type I/III ratio, and (h) qRT-PCR of MMP2/TIMP2 ratio.

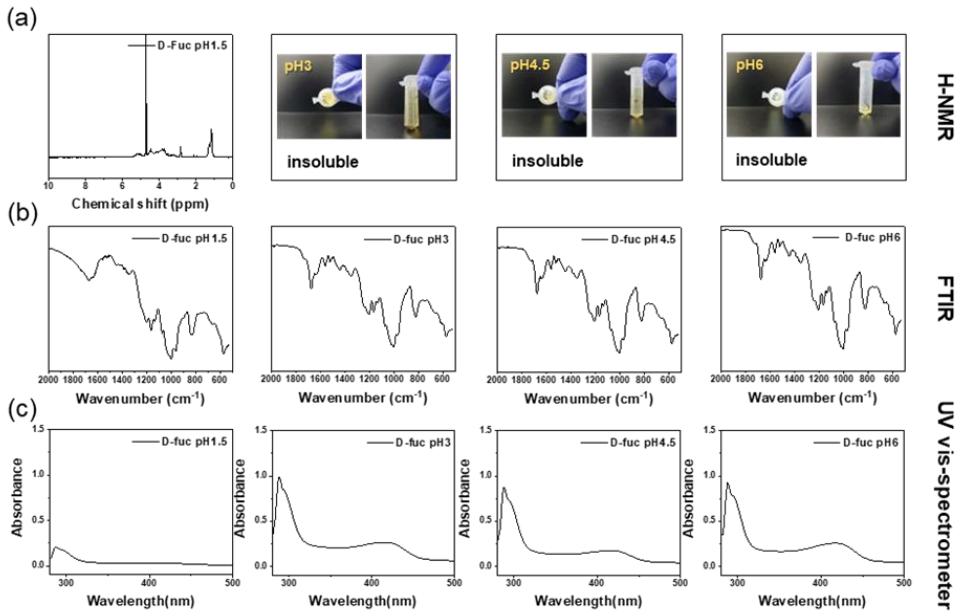

Figure S1. Optimization of DOPA conjugation to fucoidan. DOPA conjugation towards fucoidan was evaluated through deionized (DI) water with different pH. (a) ^{1}H NMR spectroscopy was not able to detect DOPA peaks on D-Fuc that was synthesized in pH 1.5. pH 3~6 allowed DOPA conjugation to fucoidan, however, they were not insoluble in DI water. (b) FTIR spectrum of D-Fuc that were conjugated in different pH environment. There were not DOPA peaks present with D-Fuc synthesized at pH 1.5, while other spectrums showed DOPA peaks of 1550 cm^{-}1 (amide II band, N-H bending) and 1650 cm^{-}1 (amide I band, C=O stretching). (c) UV-vis spectrum of D-Fuc that were conjugated in different pH environment. Similar to FTIR spectrum, DOPA peak at 280nm was present for pH 3~6, while low intensity was observed for pH 1.5. However, oxidation of DOPA occurred for D-Fuc as 400-500nm peaks represent oxidized DOPA.

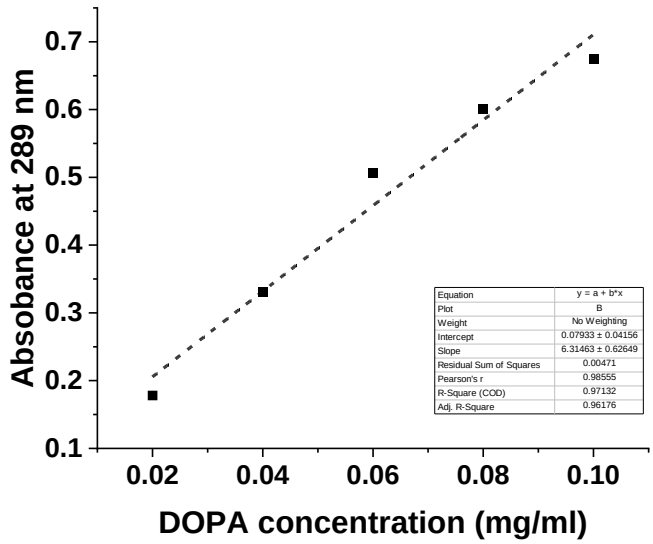

Figure S2. The calibration curve of DOPA. The standard curve of DOPA was used to quantify the DOPA conjugation rate to fucoidan.

(a)

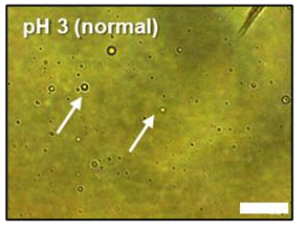

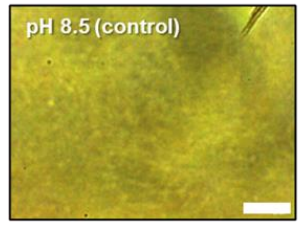

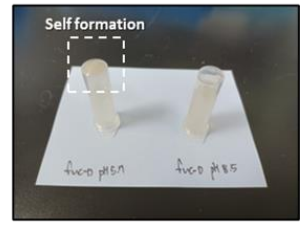

(b)

		Mixing ratio (Volume ratio)								
PBS		9	8	7	6	5	4	3	2	1
D-fuc		1	2	3	4	5	6	7	8	9
Turbidity	pH 3	0.043	0.046	0.055	0.064	0.073	0.085	0.088	0.109	0.123
	pH 7	0.037	0.052	0.073	0.064	0.076	0.093	0.115	0.098	0.095
	pH 8	0.043	0.093	0.054	0.058	0.074	0.09	0.098	0.11	0.196
	pH 8.5	-	0.036	0.035	0.035	0.036	0.035	0.037	0.038	0.037

Figure S3. Self-coacervation of D-Fuc. Self-coacervation of D-Fuc was analyzed through pH adjustment. (a) The optical microscopic images and representative photograph of D-Fuc under different pH environment. D-Fuc was dissolved in PBS and pH was adjusted by introducing NaOH. For the representative photograph, D-Fuc solutions were centrifuged at 12000 rpm for 10 min at 4 °C. (b) Turbidity of D-Fuc according to pH. D-Fuc was prepared at a concentration of 6.25 mg/ml in PBS. Turbidity was measured by a microplate reader at a wavelength of 600 nm.

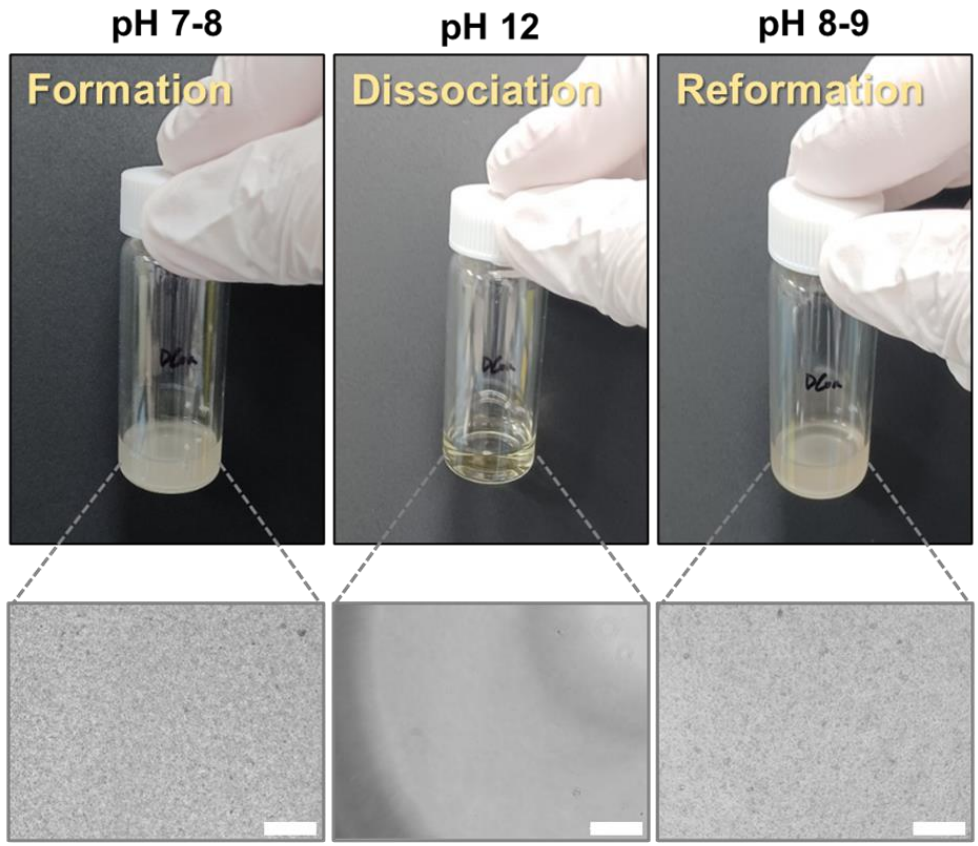

Figure S4. Reversibility of D-Coa. D-Coa dissociation and reformation was evaluated through pH adjustment. pH of the D-Coa solution instantly after coacervation was pH 7~8. When pH was increased to pH12, D-Coa dissociation was observed. Re-adjusting pH to pH 8~9 showed D-Coa reformation. Scale bar = 200 μm. pH was adjusted by introducing NaOH and HCl directly to the coacervate solution.

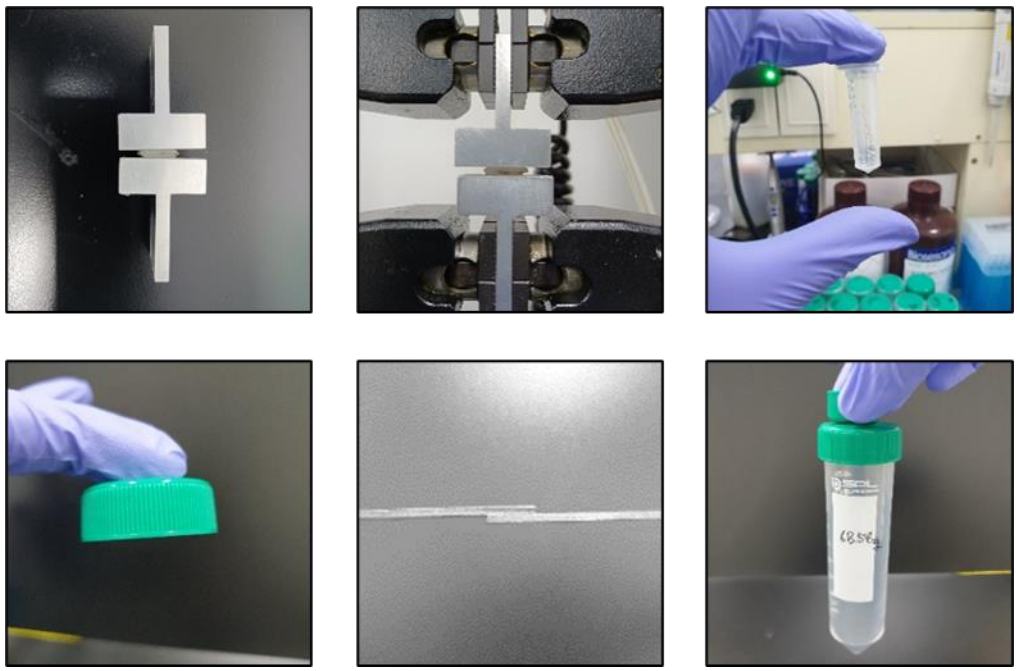

Figure S5. Adhesion ability of D-Coa on various material surfaces. D-Coa adhesive force on various materials: pig skin, metal, nitrile, polypropylene.

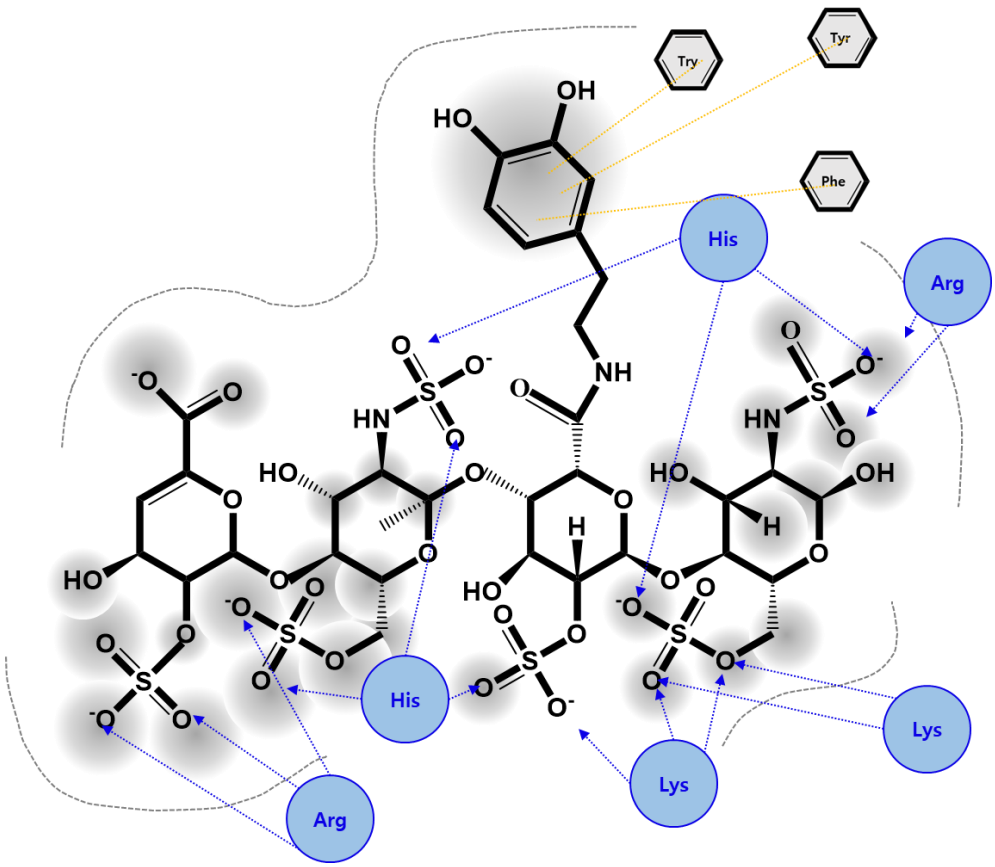

Figure S6. Illustration of interaction mechanisms between growth factors and D-Fuc. The chemical structure of fucoidan allows bonding with proteins, such as growth factors and cytokines with high affinity. Sulfate groups, a negatively charged domain, can interact with arginine, lysine, and histidine domains from growth factors. Also, phenylalanine, tyrosine, and tryptophan domains from proteins can interact with aromatic rings from DOPA. The catechol group from DOPA is also known to interact with various bonds, such as pi-pi, DOPA-DOPA, hydrogen bonds.[42, 67, 85]

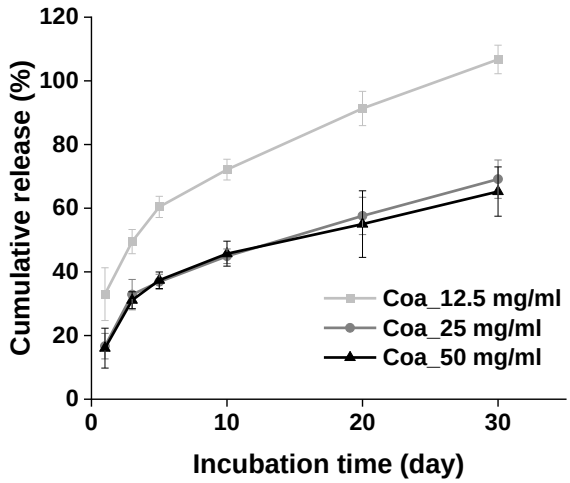

Figure S7. Cumulative release profiles of Coa with 5 min stabilization time. To evaluate the coating stabilization time of 5 min, BSA-FITC (25 ug/ml) was encapsulated in Coa with different polyelectrolyte concentrations (12.5, 25, and 50 mg/ml) (n=5). Method 1 and Fucoidan:PLL weight ratio of 50:50 (wt.%) was used. Supernatants of each time points (1, 3, 5, 10, 20, and 30 day) were collected by centrifuging the solution with 12000 rpm for 1 min at 4 ^{o}C. Then, the supernatants were measured using microplate reader (λ_{ex} : 480 λ_{em} : 530).

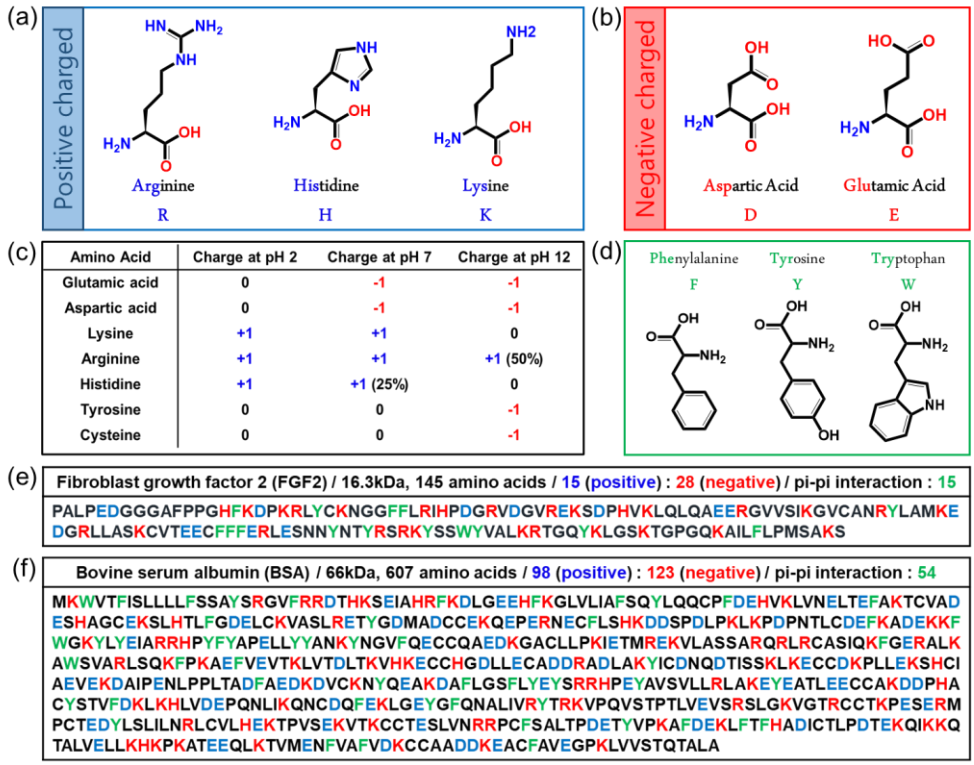

Figure S8. Amino acid sequence of BSA and FGF2 for electrostatic interaction domains. (a) Positively charged amino acids (R, H, and K). (b) Negatively charged amino acids (D and E). (c) Positively and negatively charged amino acids at different pH (acidic, neutral, and basic). (d) Specific amino acids in aromatic rings. (e & f) Amino acid sequences of FGF2 and BSA proteins.

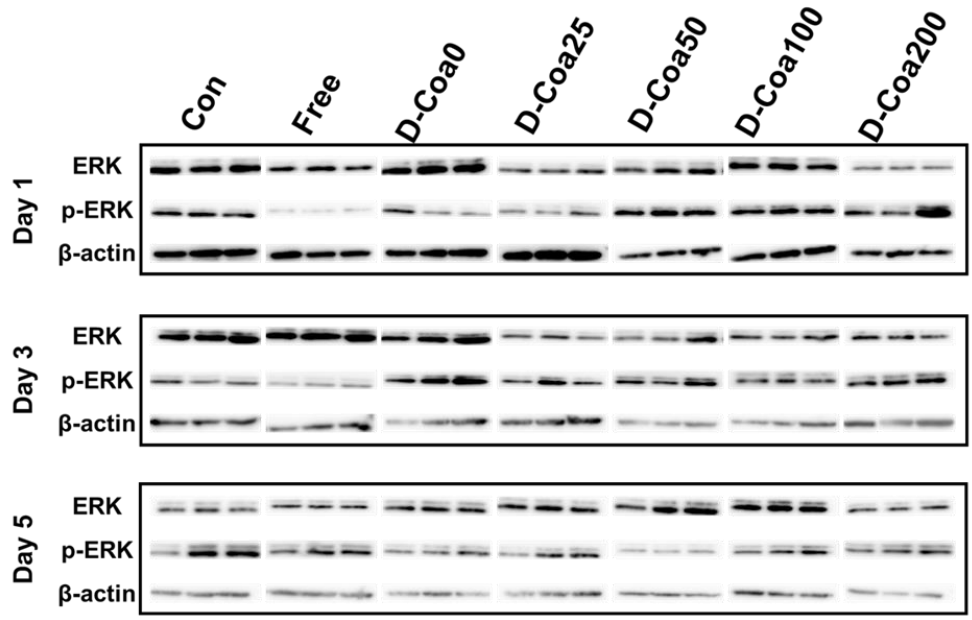

Figure S9. Sustained release of FGF2 activates ERK. Control (neat collagen sponge), free (FGF2 soaked collagen sponge), and D-Coa coated collagen sponges with various FGF2 concentrations (25, 50, 100, 200 ug/ml) were co-cultured with NIH-3T3 using a 24 well transwell plate (n=3).

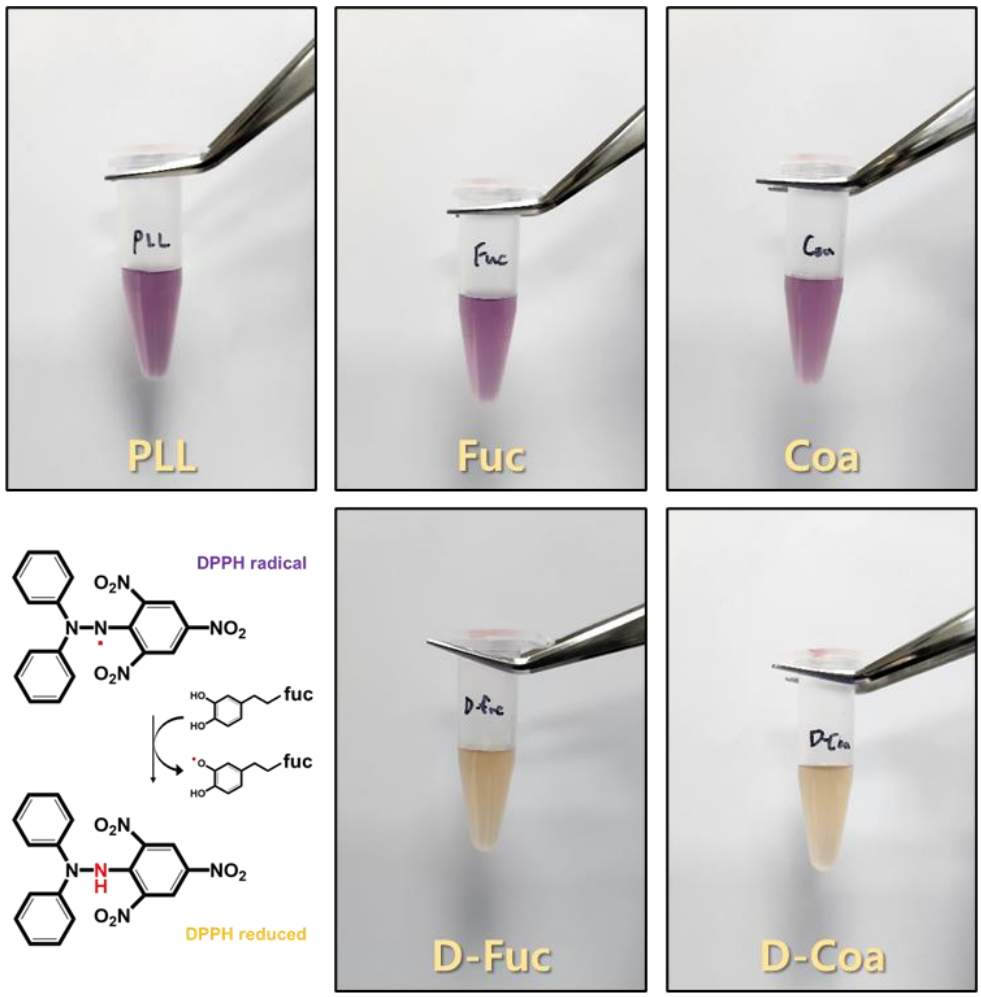

Figure S10. Antioxidant ability of D-Coa. DPPH radical (violet) was reduced by introduction of D-Fuc and D-Coa.

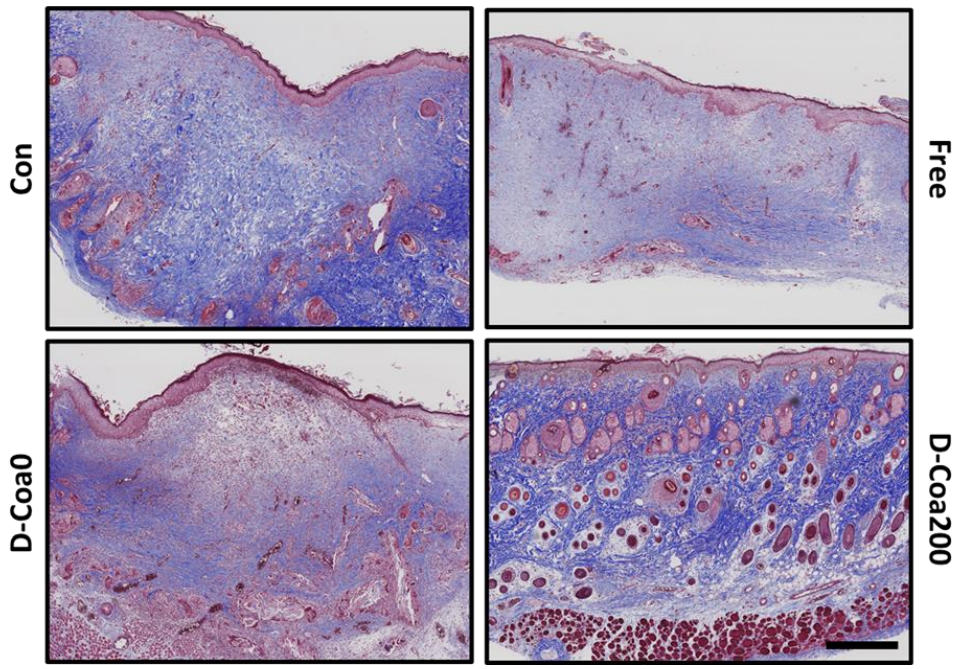

Figure S11. Histological analysis of collagen sponges. The degree of regeneration in the dermal structure after 3 weeks of post-surgery (scale bar = 1 mm).

Chapter 4. Conclusion

In summary, adhesive fucoidan/PLL complex coacervate was successfully fabricated by conjugating DOPA onto fucoidan. Adhesiveness and sustained release of FGF2 was achieved by D-Coa. The adhesive force of D-Coa was significantly increased compared to the Coa system developed from previous studies. D-Coa was able to release FGF2 in a controlled manner for 60 days, and it protected encapsulated proteins from proteolytic environment. Additionally, D-Coa was able to homogenously coat collagen sponge within 5 minutes with high FGF2 encapsulation yield. The rat excisional wound splinting model study confirmed that D-Coa coated collagen sponge was able show re-epithelialization and remodeling of dermis layer with angiogenesis and well organized collagen deposition. D-Coa is a promising adhesive and drug delivery coating material for biomedical devices. The authors believe that it can be an effective supplement for current wound healing dressing products.

References

[1] T.N. Demidova-Rice, M.R. Hamblin, I.M. Herman, Acute and Impaired Wound Healing: Pathophysiology and Current Methods for Drug Delivery, Part 1: Normal and Chronic Wounds: Biology, Causes, and Approaches to Care, Adv Skin Wound Care 25(7) (2012) 304-314.

[2] R. Laurano, M. Boffito, G. Ciardelli, V. Chiono, Wound dressing products: A translational investigation from the bench to the market, Engineered Regeneration 3(2) (2022) 182-200.

[3] M. Mirhaj, S. Labbaf, M. Tavakoli, A.M. Seifalian, Emerging treatment strategies in wound care, Int Wound J 19(7) (2022) 1934-1954.

[4] C.R. Wang, X. Jiang, H.J. Kim, S.M. Zhang, X.W. Zhou, Y. Chen, H.A. Ling, Y.M. Xue, Z.W. Chen, M.Y. Qu, L. Ren, J.X. Zhu, A. Libanori, Y.Z. Zhu, H. Kang, S. Ahadian, M.R. Dokmeci, P. Servati, X.M. He, Z. Gu, W.J. Sun, A. Khademhosseini, Flexible patch with printable and antibacterial conductive hydrogel electrodes for accelerated wound healing, Biomaterials 285 (2022).

[5] S. Guo, L.A. DiPietro, Factors Affecting Wound Healing, J Dent Res 89(3) (2010) 219-229.

[6] C.K. Sen, S. Roy, OxymiRs in cutaneous development, wound repair and regeneration, Semin Cell Dev Biol 23(9) (2012) 971-980.

[7] J.M. Reinke, H. Sorg, Wound Repair and Regeneration, Eur Surg Res 49(1) (2012) 35-43.

[8] A. Kawasumi, N. Sagawa, S. Hayashi, H. Yokoyama, K. Tamura, Wound Healing in Mammals and Amphibians: Toward Limb

Regeneration in Mammals, Curr Top Microbiol 367 (2013) 33-49.
[9] M. Rodrigues, N. Kosaric, C.A. Bonham, G.C. Gurtner, Wound Healing: A Cellular Perspective, Physiol Rev 99(1) (2019) 665-706.
[10] H.S. Kim, X.Y. Sun, J.H. Lee, H.W. Kim, X.B. Fu, K.W. Leong, Advanced drug delivery systems and artificial skin grafts for skin wound healing, Adv Drug Deliver Rev 146 (2019) 209-239.
[11] A.K. Deva, Q. Ngo, K. Vickery, Role of bacterial biofilms in chronic wounds, Wound Repair Regen 15(6) (2007) A149-A149.
[12] A.R. Siddiqui, J.M. Bernstein, Chronic wound infection: Facts and controversies, Clin Dermatol 28(5) (2010) 519-526.
[13] L. Clinton, T. Carter, Chronic Wound Biofilms: Pathogenesis and Potential Therapies, Labmedicine 46(4) (2015) 277-284.
[14] G. Han, R. Ceilley, Chronic Wound Healing: A Review of Current Management and Treatments, Adv Ther 34(3) (2017) 599-610.
[15] D. Sharma, L. Misba, A.U. Khan, Antibiotics versus biofilm: an emerging battleground in microbial communities, Antimicrob Resist In 8 (2019).
[16] J.S. Boateng, K.H. Matthews, H.N.E. Stevens, G.M. Eccleston, Wound healing dressings and drug delivery systems: A review, J Pharm Sci-Us 97(8) (2008) 2892-2923.
[17] S. Saghazadeh, C. Rinoldi, M. Schot, S.S. Kashaf, F. Sharifi, E. Jalilian, K. Nuutila, G. Giatsidis, P. Mostafalu, H. Derakhshandeh, K. Yue, W. Swieszkowski, A. Memic, A. Tamayol, A. Khademhosseini, Drug delivery systems and materials for wound healing applications, Adv Drug Deliver Rev 127 (2018) 138-166.
[18] A.K. Gaharwar, I. Singh, A. Khademhosseini, Engineered biomaterials for in situ tissue regeneration, Nat Rev Mater 5(9)

(2020) 686-705.
[19] W.C. Huang, R. Ying, W. Wang, Y.N. Guo, Y.J. He, X.Y. Mo, C.H. Xue, X.Z. Mao, A Macroporous Hydrogel Dressing with Enhanced Antibacterial and Anti-Inflammatory Capabilities for Accelerated Wound Healing, Adv Funct Mater 30(21) (2020).
[20] M. Hosseini, A. Shafiee, Engineering Bioactive Scaffolds for Skin Regeneration, Small 17(41) (2021) e2101384.
[21] S. Dhivya, V.V. Padma, E. Santhini, Wound dressings - a review, Biomedicine (Taipei) 5(4) (2015) 22.
[22] S. Chhabra, N. Chhabra, A. Kaur, N. Gupta, Wound Healing Concepts in Clinical Practice of OMFS, J Maxillofac Oral Su 16(4) (2017) 403-423.
[23] P.M. Vogt, M. Lehnhardt, D. Wagner, V. Jansen, M. Krieg, H.U. Steinau, Determination of endogenous growth factors in human wound fluid: Temporal presence and profiles of secretion, Plast Reconstr Surg 102(1) (1998) 117-123.
[24] S. Barrientos, O. Stojadinovic, M.S. Golinko, H. Brem, M. Tomic-Canic, Growth factors and cytokines in wound healing, Wound Repair Regen 16(5) (2008) 585-601.
[25] P. Tayalia, D.J. Mooney, Controlled Growth Factor Delivery for Tissue Engineering, Adv Mater 21(32-33) (2009) 3269-3285.
[26] Y.R. Yun, J.E. Won, E. Jeon, S. Lee, W. Kang, H. Jo, J.H. Jang, U.S. Shin, H.W. Kim, Fibroblast growth factors: biology, function, and application for tissue regeneration, J Tissue Eng 2010 (2010) 218142.
[27] L. Benington, G. Rajan, C. Locher, L.Y. Lim, Fibroblast Growth Factor 2-A Review of Stabilisation Approaches for Clinical Applications, Pharmaceutics 12(6) (2020).
[28] Y. Xie, N. Su, J. Yang, Q. Tan, S. Huang, M. Jin, Z. Ni, B. Zhang,

D. Zhang, F. Luo, H. Chen, X. Sun, J.Q. Feng, H. Qi, L. Chen, FGF/FGFR signaling in health and disease, Signal Transduct Target Ther 5(1) (2020) 181.

[29] S. Chakrabarti, B. Mazumder, J. Rajkonwar, M.P. Pathak, P. Patowary, P. Chattopadhyay, bFGF and collagen matrix hydrogel attenuates burn wound inflammation through activation of ERK and TRK pathway, Sci Rep-Uk 11(1) (2021).

[30] B. Behr, M. Sorkin, M. Lehnhardt, A. Renda, M.T. Longaker, N. Quarto, A Comparative Analysis of the Osteogenic Effects of BMP-2, FGF-2, and VEGFA in a Calvarial Defect Model, Tissue Eng Pt A 18(9-10) (2012) 1079-1086.

[31] M. Geiger, R.H. Li, W. Friess, Collagen sponges for bone regeneration with rhBMP-2, Adv Drug Deliver Rev 55(12) (2003) 1613-1629.

[32] F. Maisano, H.K. Kjaergard, R. Bauernschmitt, A. Pavie, G. Rabago, M. Laskar, J.P. Marstein, V. Falk, TachoSil surgical patch versus conventional haemostatic fleece material for control of bleeding in cardiovascular surgery: a randomised controlled trial, Eur J Cardio-Thorac 36(4) (2009) 708-714.

[33] A. Toro, M. Mannino, G. Reale, I. Di Carlo, TachoSil use in abdominal surgery: a review, J Blood Med 2 (2011) 31-6.

[34] Z.M. Wang, Z.F. Wang, W.W. Lu, W.X. Zhen, D.Z. Yang, S.L. Peng, Novel biomaterial strategies for controlled growth factor delivery for biomedical applications, Npg Asia Mater 9 (2017).

[35] M.E. Cam, S. Yildiz, H. Alenezi, S. Cesur, G.S. Ozcan, G. Erdemir, U. Edirisinghe, D. Akakin, D.S. Kuruca, L. Kabasakal, O. Gunduz, M. Edirisinghe, Evaluation of burst release and sustained release of pioglitazone-loaded fibrous mats on diabetic wound healing: an in vitro and in vivo comparison study, J R Soc Interface

17(162) (2020).
[36] P.S. Briquez, J.A. Hubbell, M.M. Martino, Extracellular Matrix-Inspired Growth Factor Delivery Systems for Skin Wound Healing, Adv Wound Care 4(8) (2015) 479-489.
[37] O. Saksela, D. Moscatelli, A. Sommer, D.B. Rifkin, Endothelial Cell-Derived Heparan-Sulfate Binds Basic Fibroblast Growth-Factor and Protects It from Proteolytic Degradation, J Cell Biol 107(2) (1988) 743-751.
[38] M.M. Zhao, N.S. Zacharia, Protein encapsulation via polyelectrolyte complex coacervation: Protection against protein denaturation, J Chem Phys 149(16) (2018).
[39] S. Jeong, B. Kim, H.C. Lau, A. Kim, Gelatin-Alginate Complexes for EGF Encapsulation: Effects of H-Bonding and Electrostatic Interactions, Pharmaceutics 11(10) (2019).
[40] D.H. Damon, R.R. Lobb, P.A. Damore, J.A. Wagner, Heparin Potentiates the Action of Acidic Fibroblast Growth-Factor by Prolonging Its Biological Half-Life, J Cell Physiol 138(2) (1989) 221-226.
[41] H.J. Kim, B. Yang, T.Y. Park, S. Lim, H.J. Cha, Complex coacervates based on recombinant mussel adhesive proteins: their characterization and applications, Soft Matter 13(42) (2017) 7704-7716.
[42] E.Y. Jeon, S.H. Um, J. Park, Y. Jung, C.H. Cheon, H. Jeon, J.J. Chung, Precisely Localized Bone Regeneration Mediated by Marine-Derived Microdroplets with Superior BMP-2 Binding Affinity, Small 18(24) (2022) e2200416.
[43] E.Y. Jeon, D.S. Choi, S. Choi, J.Y. Won, Y. Jo, H.B. Kim, Y. Jung, S.C. Shin, H. Min, H.W. Choi, M.S. Lee, Y. Park, J.J. Chung, H.S. Jin, Enhancing adoptive T-cell therapy with fucoidan-based

IL-2 delivery microcapsules, Bioeng Transl Med (2022).
[44] X. Wang, J. Ge, E.E. Tredget, Y. Wu, The mouse excisional wound splinting model, including applications for stem cell transplantation, Nat Protoc 8(2) (2013) 302-9.
[45] C. Zhao, S.T. Zuckerman, C. Cai, S. Kilari, A. Singh, M. Simeon, H.A. von Recum, J.N. Korley, S. Misra, Periadventitial Delivery of Simvastatin-Loaded Microparticles Attenuate Venous Neointimal Hyperplasia Associated With Arteriovenous Fistula, J Am Heart Assoc 9(24) (2020) e018418.
[46] P. Zhou, C. Yang, S. Zhang, Z.X. Ke, D.X. Chen, Y.Q. Li, Q. Li, The Imbalance of MMP-2/TIMP-2 and MMP-9/TIMP-1 Contributes to Collagen Deposition Disorder in Diabetic Non-Injured Skin, Front Endocrinol (Lausanne) 12 (2021) 734485.
[47] S. Lim, Y.S. Choi, D.G. Kang, Y.H. Song, H.J. Cha, The adhesive properties of coacervated recombinant hybrid mussel adhesive proteins, Biomaterials 31(13) (2010) 3715-22.
[48] J.H. Ryu, Y. Lee, W.H. Kong, T.G. Kim, T.G. Park, H. Lee, Catechol-functionalized chitosan/pluronic hydrogels for tissue adhesives and hemostatic materials, Biomacromolecules 12(7) (2011) 2653-9.
[49] K. Kim, K. Kim, J.H. Ryu, H. Lee, Chitosan-catechol: a polymer with long-lasting mucoadhesive properties, Biomaterials 52 (2015) 161-70.
[50] J.H. Ryu, S. Hong, H. Lee, Bio-inspired adhesive catechol-conjugated chitosan for biomedical applications: A mini review, Acta Biomaterialia 27 (2015) 101-115.
[51] C. Fan, J. Fu, W. Zhu, D.A. Wang, A mussel-inspired double-crosslinked tissue adhesive intended for internal medical use, Acta Biomater 33 (2016) 51-63.

[52] M. Rahimnejad, W. Zhong, Mussel-inspired hydrogel tissue adhesives for wound closure, RSC Adv. 7(75) (2017) 47380-47396.
[53] Y. Jeong, L.T. Thuy, S.H. Ki, S. Ko, S. Kim, W.K. Cho, J.S. Choi, S.M. Kang, Multipurpose Antifouling Coating of Solid Surfaces with the Marine-Derived Polymer Fucoidan, Macromol Biosci 18(10) (2018) e1800137.
[54] Y.K. Jo, H.J. Kim, Y. Jeong, K.I. Joo, H.J. Cha, Biomimetic Surface Engineering of Biomaterials by Using Recombinant Mussel Adhesive Proteins, Advanced Materials Interfaces 5(9) (2018).
[55] C. Cui, C. Fan, Y. Wu, M. Xiao, T. Wu, D. Zhang, X. Chen, B. Liu, Z. Xu, B. Qu, W. Liu, Water-Triggered Hyperbranched Polymer Universal Adhesives: From Strong Underwater Adhesion to Rapid Sealing Hemostasis, Adv Mater 31(49) (2019) e1905761.
[56] Q. Guo, J. Chen, J. Wang, H. Zeng, J. Yu, Recent progress in synthesis and application of mussel-inspired adhesives, Nanoscale 12(3) (2020) 1307-1324.
[57] Y. Li, J. Cheng, P. Delparastan, H. Wang, S.J. Sigg, K.G. DeFrates, Y. Cao, P.B. Messersmith, Molecular design principles of Lysine-DOPA wet adhesion, Nat Commun 11(1) (2020) 3895.
[58] Q. Peng, J. Chen, Z. Zeng, T. Wang, L. Xiang, X. Peng, J. Liu, H. Zeng, Adhesive Coacervates Driven by Hydrogen-Bonding Interaction, Small 16(43) (2020) e2004132.
[59] M. Shin, J.Y. Shin, K. Kim, B. Yang, J.W. Han, N.K. Kim, H.J. Cha, The position of lysine controls the catechol-mediated surface adhesion and cohesion in underwater mussel adhesion, J Colloid Interface Sci 563 (2020) 168-176.
[60] P. Zhao, X. Xia, X. Xu, K.K.C. Leung, A. Rai, Y. Deng, B. Yang, H. Lai, X. Peng, P. Shi, H. Zhang, P.W.Y. Chiu, L. Bian,

Nanoparticle-assembled bioadhesive coacervate coating with prolonged gastrointestinal retention for inflammatory bowel disease therapy, Nat Commun 12(1) (2021) 7162.
[61] M. Cencer, Y. Liu, A. Winter, M. Murley, H. Meng, B.P. Lee, Effect of pH on the rate of curing and bioadhesive properties of dopamine functionalized poly(ethylene glycol) hydrogels, Biomacromolecules 15(8) (2014) 2861-9.
[62] Y. Kan, E.W. Danner, J.N. Israelachvili, Y. Chen, J.H. Waite, Boronate complex formation with Dopa containing mussel adhesive protein retards ph-induced oxidation and enables adhesion to mica, PLoS One 9(10) (2014) e108869.
[63] L. Li, B. Yan, J. Yang, L. Chen, H. Zeng, Novel mussel-inspired injectable self-healing hydrogel with anti-biofouling property, Adv Mater 27(7) (2015) 1294-9.
[64] Z. Wang, S. Zhang, S. Zhao, H. Kang, Z. Wang, C. Xia, Y. Yu, J. Li, Facile biomimetic self-coacervation of tannic acid and polycation: Tough and wide pH range of underwater adhesives, Chemical Engineering Journal 404 (2021).
[65] J. Pathak, E. Priyadarshini, K. Rawat, H.B. Bohidar, Complex coacervation in charge complementary biopolymers: Electrostatic versus surface patch binding, Adv Colloid Interfac 250 (2017) 40-53.
[66] A.P. Imeson, D.A. Ledward, J.R. Mitchell, On the nature of the interaction between some anionic polysaccharides and proteins, Journal of the Science of Food and Agriculture 28(8) (1977) 661-668.
[67] N.S. Gandhi, R.L. Mancera, The Structure of Glycosaminoglycans and their Interactions with Proteins, Chem Biol Drug Des 72(6) (2008) 455-482.

[68] K.A. Black, D. Priftis, S.L. Perry, J. Yip, W.Y. Byun, M. Tirrell, Protein Encapsulation via Polypeptide Complex Coacervation, Acs Macro Lett 3(10) (2014) 1088−1091.
[69] N.J. Zondlo, Aromatic−proline interactions: electronically tunable CH/pi interactions, Acc Chem Res 46(4) (2013) 1039−49.
[70] P.K. Forooshani, B.P. Lee, Recent approaches in designing bioadhesive materials inspired by mussel adhesive protein, J Polym Sci Pol Chem 55(1) (2017) 9−33.
[71] W.C. Lim, H. Kim, Y.J. Kim, B.N. Jeon, H.B. Kang, H. Ko, Catechol inhibits epidermal growth factor−induced epithelial−to−mesenchymal transition and stem cell−like properties in hepatocellular carcinoma cells, Sci Rep−Uk 10(1) (2020).
[72] J. Wu, J.J. Ye, J.J. Zhu, Z.C. Xiao, C.C. He, H.X. Shi, Y.D. Wang, C. Ling, H.Y. Zhang, Y.Z. Zhao, X.B. Fu, H. Chen, X.K. Li, L. Li, J. Zheng, J. Xiao, Heparin−Based Coacervate of FGF2 Improves Dermal Regeneration by Asserting a Synergistic Role with Cell Proliferation and Endogenous Facilitated VEGF for Cutaneous Wound Healing, Biomacromolecules 17(6) (2016) 2168−2177.
[73] M. Farooq, A.W. Khan, M.S. Kim, S. Choi, The Role of Fibroblast Growth Factor (FGF) Signaling in Tissue Repair and Regeneration, Cells−Basel 10(11) (2021).
[74] S. Zafar, R. Ahmed, R. Khan, Biotransformation: a green and efficient way of antioxidant synthesis, Free Radical Res 50(9) (2016) 939−948.
[75] D. Zhou, S.Z. Li, M.J. Pei, H.J. Yang, S.J. Gu, Y.Z. Tao, D.Z. Ye, Y.S. Zhou, W.L. Xu, P. Xiao, Dopamine−Modified Hyaluronic Acid Hydrogel Adhesives with Fast−Forming and High Tissue Adhesion, Acs Appl Mater Inter 12(16) (2020) 18225−18234.
[76] B. Kim, Y. Kim, Y. Lee, J. Oh, Y. Jung, W.G. Koh, J.J. Chung,

Reactive Oxygen Species Suppressive Kraft Lignin-Gelatin Antioxidant Hydrogels for Chronic Wound Repair, Macromolecular Bioscience 22(11) (2022).
[77] C. Dunnill, T. Patton, J. Brennan, J. Barrett, M. Dryden, J. Cooke, D. Leaper, N.T. Georgopoulos, Reactive oxygen species (ROS) and wound healing: the functional role of ROS and emerging ROS-modulating technologies for augmentation of the healing process, Int Wound J 14(1) (2017) 89-96.
[78] M.G. Tonnesen, X. Feng, R.A. Clark, Angiogenesis in wound healing, J Investig Dermatol Symp Proc 5(1) (2000) 40-6.
[79] M. Miyoshi, T. Kawazoe, H.H. Igawa, Y. Tabata, Y. Ikada, S. Suzuki, Effects of bFGF incorporated into a gelatin sheet on wound healing, J Biomat Sci-Polym E 16(7) (2005) 893-907.
[80] L.E. Tracy, R.A. Minasian, E.J. Caterson, Extracellular Matrix and Dermal Fibroblast Function in the Healing Wound, Adv Wound Care (New Rochelle) 5(3) (2016) 119-136.
[81] E.A. Lenselink, Role of fibronectin in normal wound healing, Int Wound J 12(3) (2015) 313-6.
[82] D. Greiling, R.A. Clark, Fibronectin provides a conduit for fibroblast transmigration from collagenous stroma into fibrin clot provisional matrix, J Cell Sci 110 (Pt 7) (1997) 861-70.
[83] F. Shi, J. Harman, K. Fujiwara, J. Sottile, Collagen I matrix turnover is regulated by fibronectin polymerization, Am J Physiol-Cell Ph 298(5) (2010) C1265-C1275.
[84] D.E. Birk, R. Mayne, Localization of collagen types I, III and V during tendon development. Changes in collagen types I and III are correlated with changes in fibril diameter, Eur J Cell Biol 72(4) (1997) 352-61.
[85] D. Hachim, T.E. Whittaker, H. Kim, M.M. Stevens,

Glycosaminoglycan-based biomaterials for growth factor and cytokine delivery: Making the right choices, J Control Release 313 (2019) 131-147.

국문초록

상처 드레싱을 위한 생활성 코팅 보조제로서의 접착성 코아세르베이트

김 영
응용바이오공학과
서울대학교 융합과학기술대학원

코아세르베이트 (coacervate)는 서로 반대되는 전하를 갖는 고분자가 수용액에서 만나 상호작용하여 순전하 0을 형성하면서 액체-액체 상분리 또는 액체 방울의 형성되는 것을 의미한다. 식품 첨가물부터 생명공학까지 다양한 연구 분야에 코아세르베이트가 적용되고 있다. 이전 연구에서 해양 유래 글라이코사미노글라이칸 (glycosaminoglycan)인 후코이단 (fucoidan)과 폴라라이신 (poly-*l*-lysine)을 이용한 코아세르베이트는 암 면역 요법과 조직 공학 응용을 위해 지속적인 방출 프로파일, 우수한 탑재 능력, 생체 적합성 및 가혹한 (harsh) 생체 내 환경으로부터의 보호와 같은 특성을 보여주었다. 또한 약물 전달체로서 단백질 방출을 보여주었다.

본 연구에서는, 기존의 상처 치유를 위한 패치를 뛰어넘기 위해 후코이단을 도파민으로 기능화하여 접착성 코아세르베이트를 합성하였다. 도파가 붙은 후코이단과 폴라 라이신의 코아세르베이트는 콜라겐 스펀지에 균일하고 빠르게 성공적으로 코팅되었다. 코아세르베이트 코팅 콜라겐 스펀지는 섬유아세포 성장인자를 탑재하여 지속적으로 방출할 수 있었고, 효소로부터 보호 능력을 보였다. 쥐를 이용한 피부 결함 모델에서, 접착성 코아세르베이트를 코팅한 패치를 이용함으로써 성공적인 상처 재생 효과를 입증하였다. 도파-코아세르베이트 코팅은

운드 재생 분야를 위한 유망한 접착 물질이다.